

## Research Paper

## Experimental research on mechanised strip application process based on DEM of compressed granulated straw



Guibin Chen<sup>a,b,\*</sup>, Jiaming Yang<sup>c</sup>, Fuzeng Yang<sup>a,b</sup>, Qingjie Wang<sup>d</sup>, Zhijie Liu<sup>a,b</sup>, Zhengdao Liu<sup>a,\*\*</sup>

<sup>a</sup> College of Mechanical and Electronic Engineering, Northwest A&F University, Yangling, 712100, China

<sup>b</sup> Scientific Observation and Experimental Station of Agricultural Equipment for the Northern China Ministry of Agriculture and Rural Affairs, Yangling, 712100, China

<sup>c</sup> College of Forestry, Northwest A&F University, Yangling, 712100, China

<sup>d</sup> College of Engineering, China Agricultural University, Beijing, 100083, China

## ARTICLE INFO

## Keywords:

Conservation agriculture  
Strip tillage  
DEM  
Counter roller  
Granulated straw

## ABSTRACT

Returning the entire straw to the field can lead to excessive buildup, obstructing the seeding process and reducing quality. To address this, technologies like straw granulation and strip application enhance straw decomposition and soil organic matter. However, differing sizes of granulated straw can impact seeding quality. This paper presents a straw-crushing device with a differential counter roller that breaks long straw particles during rotation. It also includes trenching shovels, covering discs, and compaction wheels for practical mechanised application. The discrete element method (DEM) was used to simulate the straw crushing capacity and analyse the factors affecting the crushing rate. The work determined that the centre distance between the two rollers is 99 mm, the teeth height  $H$  is 15 mm, teeth width  $b_1$  is 10 mm, and teeth thickness  $b_2$  is 10 mm. It was found that the minimal variation in the straw crushing rate varied between 0.77 and 1.77 kg s<sup>-1</sup>. Optimal crushing rates are achieved when the upper roller's rotation speed ranges from 100 to 200 r·min<sup>-1</sup> and the lower roller's speed ranges from 300 to 400 r·min<sup>-1</sup>. A simulation model is also developed to analyse the mechanised strip application process. Through single-factor tests and orthogonal test methods, the operational parameters were optimised. The findings indicated that an upper roller speed of 150 r·min<sup>-1</sup>, a lower roller speed of 300 r·min<sup>-1</sup>, a strip application depth of 150 mm, and a forward speed of 5 km h<sup>-1</sup> resulted in a straw crushing rate of 33.6 %. The uniformity variation coefficient of strip application is determined to be 14.4 %, which complies with the strip application requirements. Field validation of the test parameters yielded an average coefficient of variation of 14.9 %; the average crushing rate of granulated straw is 41.5 %, with an error margin of 0.5 % and 7.9 % compared to field tests. The optimised parameters achieve the necessary standards for mechanised strip application, providing valuable technical support for developing new granulated straw strip application methodologies.

## Nomenclature

(continued)

A	the normal stiffness per unit area and shear stiffness per unit area values of the normal bond
B	the normal strength and shear strength values of the normal bond
$b_1$	teeth width, mm
$b_2$	teeth thickness, mm
BB	Box-Behnken

(continued on next column)

C	the normal stiffness per unit area and shear stiffness per unit area values of the tangential bond
D	the normal strength and shear strength values of the tangential bond
d	roller diameter, mm
$D_1$	the major diameter of the roller, mm
DEM	Discrete Element Method
$E_1$	the elastic modulus of the straw, Pa
F	the normal force acting on the straw, N

(continued on next page)

This article is part of a special issue entitled: DEM for Agricultural & Biological Systems published in Biosystems Engineering.

\* Corresponding author. College of Mechanical and Electronic Engineering, Northwest A&F University, Yangling, 712100, China.

\*\* Corresponding author.

E-mail addresses: [chenguibin@nwsuaf.edu.cn](mailto:chenguibin@nwsuaf.edu.cn) (G. Chen), [liuzd@nwsuaf.edu.cn](mailto:liuzd@nwsuaf.edu.cn) (Z. Liu).

<https://doi.org/10.1016/j.biosystemseng.2025.104274>

Received 27 March 2025; Received in revised form 28 August 2025; Accepted 31 August 2025

Available online 5 September 2025

1537-5110/© 2025 IAgE. Published by Elsevier Ltd. All rights are reserved, including those for text and data mining, AI training, and similar technologies.

(continued)

$F_A$	the crushing force of the upper roller teeth on the straw, N
$F_B$	the normal force of the lower roller teeth on the straw, N
$F_{e1}$	the biting force exerted by the upper roller teeth on the straw, N
$F_{e2}$	the biting force exerted by the lower roller teeth on the straw, N
$F_f 1$	the frictional force between the upper roller teeth and the straw, N
$F_f 2$	the frictional force between the lower roller teeth and the straw, N
$F_{r1}$	the normal force exerted by the upper roller teeth on the straw, N
$F_{r2}$	the normal force exerted by the lower roller teeth on the straw, N
$H$	teeth height, mm
$l$	straw length, mm
$P$	the motor power, kW
$q_n$	crushing rate, (%)
$R$	the distance from the teeth tip to the centre, mm
$R_i$	the wall thickness of the roller, mm
$r$	the radius of the straw, mm
$S$	the distance between adjacent teeth within the cross-section, mm
$U$	the energy required for crushing granulated straw, kW
$\alpha, \delta$	the bite angles of the upper and lower roller teeth, (°)
$\beta_0$	friction angle between straw and roller teeth, (°)
$\kappa_1, \kappa_2$	proportional coefficient
$\mu$	length proportionality coefficient
$\rho$	the density of the roller material, g·cm <sup>-3</sup>
$\sigma_{\max}$	the strength limit of the straw, Pa
$\chi$	minimum diameter correction factor

## 1. Introduction

The total amount of straw returned to the field is conducive to the rapid improvement of soil organic matter. However, the traditional method of straw returned to the field leads to a large amount of straw on the ground, adversely affecting sowing (Hou et al., 2022; Torotwa et al., 2021). Compression granulated straw mechanised strip application is a new way of straw returning to the field, which can increase the soil organic matter content, improve soil structure, and improve soil fertility and moisture conservation. At the same time, it can reduce the amount of straw mulch on the ground and avoid the problems of poor seedling quality and easy occurrence of pests (Wang et al., 2015, 2023). However, the length distribution of straw particles could be more consistent in the preparation process of compressed granulated straw. In the process of mechanised strip application, the length of the straw is too long, and the seeds are easily in contact with the long straw directly, which affects the quality of subsequent seeding and emergence (Liu et al., 2010, 2023).

Ground spraying and mechanised strip application are two ways of returning compressed granulated straws to the field. Among them, applying straw strips to the sub-surface of soil can accelerate the decomposition rate of straw and reduce the amount of straw coverage on the surface (Tong et al., 2023). The higher the degree of straw fineness in the process of strip application, the smaller the impact on subsequent sowing and emergence (Li et al., 2022; Ucgul et al., 2018). In Northeast China, straw granulation has been partly popularised and applied. However, the need for more relevant research on mechanised strip application equipment has greatly limited the development of straw granulation. Scholars have studied straw before returning to the field. Using finite element and discrete element methods (DEM) to build an accurate numerical model of compressed straw and by simulating the interaction between straw and crushing, cleaning, mixing, and burying devices, optimising the design of key parts of straw contact is a more practical design method (Aikins, Ucgul, et al., 2021; Barr et al., 2020). In constructing a discrete element model of straw, Tang et al. (2023) studied the influence of vibration conditions and straw length on the compression quality. Shi et al. (2023) constructed a biaxially anisotropic flexible wheat straw model to simulate the mechanical properties of compression, bending, and shear. Leblcq et al. (2016) simulated the compression characteristics of straw based on the combination of the actual deformation state and the minimum model parameters. Lenaerts et al. (2014) established the DEM segmented bendable straw, but did not

consider the differential shear effect in the crushing process. Shaikh et al. (2021) analysed the interaction between components and cohesive soil, providing a reference for the contact model between granular materials and machinery. In terms of simulating straw crushing, Li et al. (2024) established the coupling interaction model of the straw crushing device and flexible straw to accurately evaluate the stubble cleaning performance.

Regarding simulating straw cleaning, Zhao et al. (2020) designed three types of straw cleaning tools for straw mulching and returning to the field, optimising and verifying them through discrete element rigid straw simulation and soil tank test. Hou et al. (2022) designed a straw-cleaning device based on active rotation. Regarding simulating straw mixing, Zhu et al. (2023) analysed the rice straw rotary tillage process by combining finite element and discrete element methods. They verified it based on a soil tank test. Lin et al. (2024) established the interaction model of rice straw and spade seedbed preparation device, providing a reference for improving the distribution uniformity of rice straw in soil. Tong et al. (2023) designed a straw-picking, injecting, and burying combined operation machine to reduce the amount of straw on the ground. In terms of simulating the impact of straw on agricultural machinery walking, Xie et al. (2024) built an interaction model between agricultural machinery walking devices and flexible straws, providing support for the structural optimisation of walking devices and tillage machinery. The above research provides technical support for mechanised strip application of compressed and dense straws.

In conclusion, the advancement of simulation technology has led to the evolution of straw modelling from rigid to flexible (Shi et al., 2023; Zhang et al., 2023). Flexible straw modelling allows for the simulation of mechanical properties such as deformation and fracture resulting from force on the straw. In the process of granulated straw strip application, the traditional crushing method of high-speed rotating parts is unsuitable. Straw particles easily collide with the cutter violently, which will damage the cutter and cause a poor crushing effect (Lee et al., 2003; Matin et al., 2016). This research and the development of the device, along with the optimisation of operating parameters, can provide essential technical and equipment support for new methods of returning straw to the field.

## 2. Materials and methods

### 2.1. Structure of straw crushing device with differential counter roller

Applying compressed straw strips into the soil can accelerate straw decomposition. During the preparation of granulated straw, the straw particle length is uneven, and the straw length is too long, which makes it challenging to rot and affects seed emergence in the process of mechanised strip application. Therefore, a differential roller-type straw particle crushing device was designed to complete the granulated straw crushing strip application (Fig. 1a).

The mechanised strip application process of straw can be divided into the following three processes: I. The rotation speed of the chain row and the opening of the baffle control the flow of the granulated straw. II. The inner teeth of the ring die, and the outer teeth of the counter roll mesh with each other, and the crushed straw is extruded by rolling to form high-density compressed straw particles. III. The differential rotation of the roller strip applicator will mesh and break the long straw particles through the differential rotation between the roller teeth (Fig. 1b).

### 2.2. Structural parameters and spatial layout of roller crushing device

The structural parameters and spatial arrangement of the roller have a direct impact on the crushing of granulated straw. In this paper, the parameters such as teeth profile, toothed roller, roller teeth distribution, and roller spatial arrangement are determined through theoretical analysis.

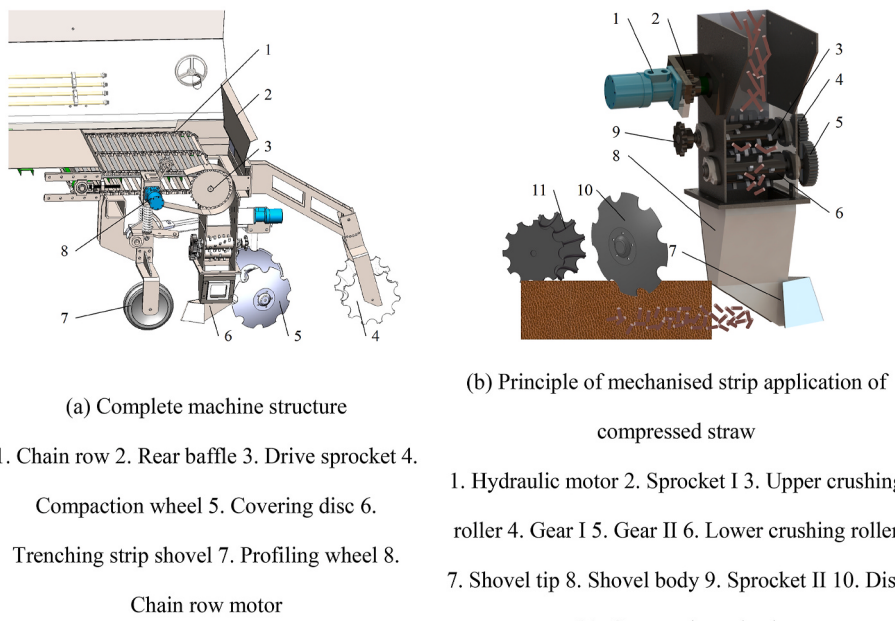


**Fig. 1.** Mechanised strip application process of compressed granulated straw.

### 2.2.1. Parameters of teeth structure

In the design process of the roll crushing device, in order to make the granulated straw fully broken, the structural forms such as discontinuous strip teeth, continuous strip teeth, and combined crushing teeth were considered in the preliminary study. The theoretical analysis and pre-test of the three types of teeth structure were carried out. The results showed that the continuous strip adjacent to two teeth made it easy to clip the granulated straw in the middle, reducing the crushing effect and other defects. The combined crushing teeth also had the adjacent roller teeth gap blocking the straw. Through the comparative test, we selected the discontinuous strip teeth structure as the preliminary structure of the straw crushing device.

The teeth height  $H$  is positively correlated with the crushing ratio, and a lower crushing ratio requires a smaller teeth height to achieve the desired crushing effect. In order to ensure that the granulated straw is fully sheared and squeezed by the roller teeth, it is necessary to consider the coordinated design of the teeth height  $H$ , teeth width  $b_1$ , and teeth thickness  $b_2$ . The  $b_1$  and  $b_2$  directly affect the feeding capacity, crushing efficiency, and wear life of granulated straw. According to empirical Eq. (1):

$$\left\{ \begin{array}{l} \frac{l_2}{2} \leq H \leq l_2 \\ b_1 = H \times \kappa_1 \\ b_2 = H \times \kappa_2 \end{array} \right. \quad (1)$$

where,  $H$ -teeth height, mm;  $b_1$ -teeth width, mm;  $b_2$ -teeth thickness, mm;  $\kappa_1, \kappa_2$ -proportional coefficient, taken as 0.67; result that  $H$  is 15 mm,  $b_1$  is 10 mm,  $b_2$  is 10 mm.

### 2.2.2. Structural parameters of toothed roller

The test material is granulated straw, which has differences in mechanical properties between normal and tangential directions. In order to improve its crushing performance, the wall thickness  $R_i$  of the roller is a constant value, and the mass  $m$ , diameter  $d$ , and shaft length  $l$  of the crushing roller are determined according to Eq. (2).

$$\left\{ \begin{array}{l} m = \frac{\pi d^2 - \pi(d - 2R_i)^2}{4} \rho l \\ d = \frac{q_n \phi}{\chi \sin^2 \beta_0} \\ l = \frac{d}{u} \end{array} \right. \quad (2)$$

where,  $\rho$ -the density of the roller material,  $\text{g}\cdot\text{cm}^{-3}$ ;  $q_n$ -crushing rate, taken as 0.68;  $\beta_0$ -friction angle between straw and roller teeth, generally taken as  $30^\circ$ ;  $\chi$ -minimum diameter correction factor;  $l$ -shaft length;  $u$ -length proportionality coefficient. Finally, the length of the roller was determined to be 170 mm.

### 2.2.3. Roller teeth arrangement and determination of relative position to rollers

To ensure that the straw crushing length meets the requirements and that the crushing teeth are firmer when biting into the straw, the spacing  $s$  between adjacent teeth in the section is twice the length of the straw. Calculate the number of roller teeth in the section according to Eq. (3):

$$N = \frac{\pi(D_1 - 2H)}{S} \quad (3)$$

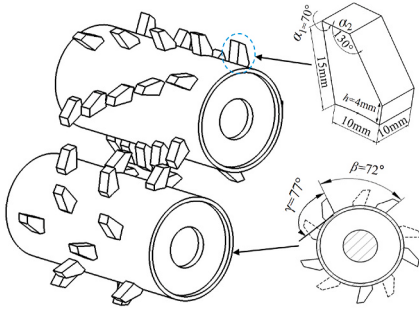
where,  $D_1$ -the major diameter of the roller, mm;  $S$ - the distance between adjacent teeth within the cross-section, mm.

If the straw size is required to be below 40 mm, then  $S$  takes 50 mm to meet the requirement. Therefore, the pitch  $p$  between adjacent roller teeth is determined to be 45 mm, and the final calculation is rounded to  $N = 5$  (Fig. 2b). To ensure the crushing effect of the roller teeth and improve their ability, the elevation angle is designed to be  $\gamma = 77^\circ$  (Fig. 2a).

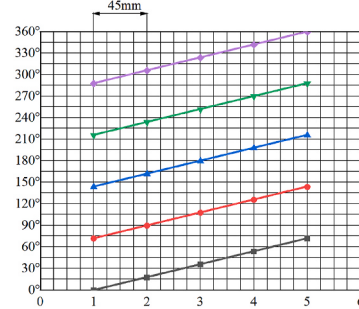
When the centre distance is small, the friction and extrusion force between the roller shaft and the granulated straw increase, which will accelerate the wear of the roller shaft surface. When the centre distance is large, it leads to insufficient material crushing and requires secondary crushing. The centre distance  $a$  should satisfy Eq. (4):

$$H + d \leq a \leq 2H + d \quad (4)$$

During the theoretical analysis process, when the centre distance



(a) Structural parameters of roller teeth



(b) Axial arrangement of roller teeth

Fig. 2. Installation parameters and structural parameters of rollers.

between the two rollers is 91 mm, the teeth of the rollers are tangent to each other. When the centre distance is 106 mm, the roller teeth touch the cylinder wall. When the final intermediate value  $a$  is 99 mm, there is moderate overlap in the working area of the roller teeth, and the crushing effect is better. Other installation parameters are shown in Fig. 3.

#### 2.2.4. Theoretical analysis of interaction process between crushing roller and straw

The roller surface bites, feeds the granulated straw, and crushes it. The entire process is very complex, and it is important to clarify the working parameters such as the crushing force on the granulated straw and the speed of the crushing roller to improve the quality of the granulated straw crushing strip. A simplified force crushing model for granulated straw is shown in Fig. 4.

At the moment when teeth  $A$  and  $B$  bite into the material during the crushing process, according to the static equilibrium equation, the crushing force of roller teeth  $A$  and  $B$  is given by Eq. (5).

$$\begin{cases} F_{r1} = F_A \sin \delta \\ F_{e1} = F_A \cos \delta \\ F_{r2} = F_B \sin \alpha \\ F_{e2} = F_B \cos \alpha \end{cases} \quad (5)$$

where  $F_A$  is the crushing force of the upper roller teeth on the straw, N;  $F_B$  is the normal force of the lower roller teeth on the straw, N;  $F_{r1}$  is the normal force exerted by the upper roller teeth on the straw, N;  $F_{r2}$  is the normal force exerted by the lower roller teeth on the straw, N;  $F_{e1}$  is the biting force exerted by the upper roller teeth on the straw, N;  $F_{e2}$  is the biting force exerted by the lower roller teeth on the straw, N;  $\alpha, \delta$  are the bite angles of the upper and lower roller teeth, ( $^{\circ}$ ).

In order to achieve non-relative sliding crushing between straw and

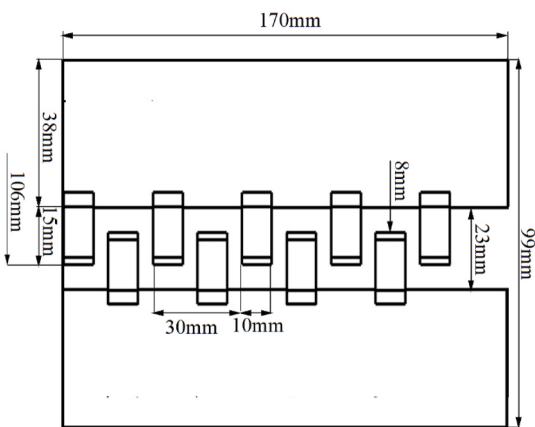


Fig. 3. Installation and spatial layout of rollers.

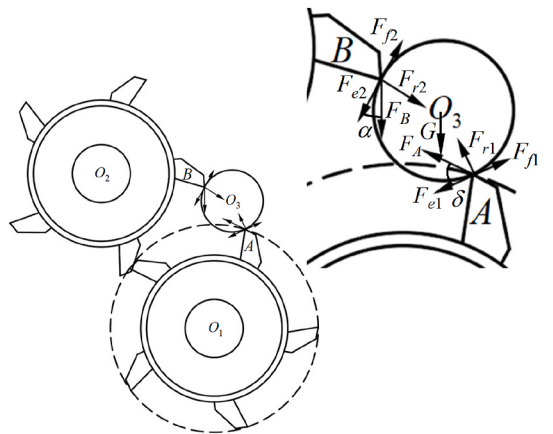


Fig. 4. Theoretical analysis of the interaction process between the crushing roller and straw.

roller teeth, Eq. (6) needs to be satisfied.

$$\begin{cases} F_{f1} \sin \alpha \leq F_{f2} \sin \delta \\ F_{f1} = \mu F_A \\ F_{f2} = \mu F_B \end{cases} \quad (6)$$

$F_{f1}$  is the frictional force between the upper roller teeth and the straw, N;  $F_{f2}$  is the frictional force between the lower roller teeth and the straw, N;  $\mu$  is the friction coefficient between the straw and the roller teeth.

During the process of straw crushing, the local area is first impacted and enters a broken state. When the particle radius decreases by  $\Delta r$ , the granulated straw must satisfy Eq. (7) between the work  $W$  done by the crushing roller and the required energy  $U$ .

$$\begin{cases} W \geq U \\ W = F_{r1} \Delta r + F_{r2} \Delta r \\ U = \int_l^F \frac{F^2}{2E_1 A_1} dx = \frac{2\pi\sigma_{\max}^2}{3E_1} [r^3 - (r - \Delta r)^3] \end{cases} \quad (7)$$

where  $F$  is the normal force acting on the straw, N;  $E_1$  is the elastic modulus of the straw, Pa;  $A_1$  is the stress area of the straw,  $m^2$ ;  $\sigma_{\max}$  is the strength limit of the straw, Pa;  $U$  is the energy required for crushing granulated straw, kW;  $r$  is the radius of the straw, mm.

According to Eq. (8), the higher the crushing rate of straw particles, the greater the energy required, and vice versa, the lower the energy required.

$$\begin{cases} \max(F_r + F_{r2}) = \lim_{\Delta r \rightarrow 0} \left[ \frac{2\pi\sigma_{\max}^2}{3E_1} \frac{r^3 - (r - \Delta r)^3}{\Delta r} \right] = \frac{2\pi\sigma_{\max}^2}{E} \\ \min(F_A + F_B) = \frac{\pi\sigma_{\max}^2 r^2}{E_1 \sin \alpha} + \frac{\pi\sigma_{\max}^2 r^2}{E_1 \sin \delta} \end{cases} \quad (8)$$

The minimum crushing force required for straw crushing is mainly influenced by the diameter and bite position of the straw, as determined by force analysis. The crushing force is positively correlated with the particle size distribution of straw, and the structural parameters and bite angle of the roller teeth determine the bite position. After the roller teeth structure parameters are determined, the larger the bite angle, the smaller the minimum crushing force. The roller teeth are driven by a synchronous motor connected to a coupling, with a motor (XD-5D120GN-C) power of 120 W. The combined equations are obtained according to the motor torque Eq. (9).

$$\frac{\pi R r^2 \sigma_{\max}^2}{9550PE_1} \left( \frac{1}{\sin \alpha} + \frac{1}{\sin \delta} \right) \leq \left( \frac{1}{n_1} + \frac{1}{n_2} \right) \leq \frac{2\pi R \sigma_{\max}^2}{9550PE_1} \quad (9)$$

where  $R$  is the distance from the teeth tip to the centre, mm;  $P$  is the motor power, kW.

Additional shear force is applied to the straw during crushing, causing a change in the type of straw crushing. At the same time, the differential speed ratio determines the relative movement speed of the straw between the two rollers, thereby changing the proportion of shear and compression effects, Eq. (10). Therefore, it is necessary to introduce strength limit correction coefficients  $\lambda_1$  and  $\lambda_2$ .

$$\frac{\pi R r^2 (\lambda_1 \sigma_{\max})^2}{9550PE_1} \left( \frac{1}{\sin \alpha} + \frac{1}{\sin \delta} \right) \leq \left( \frac{1}{n_1} + \frac{1}{n_2} \right) \leq \frac{2\pi R (\lambda_2 \sigma_{\max})^2}{9550PE_1} \quad (10)$$

The preliminary determination is that the ratio of the differential speed between the upper and lower roller teeth is within the range of 1:3; Take 1.5 GPa for  $E$ ;  $R$  is taken as 53 mm;  $r$  is taken as 35.6 mm;  $\alpha$  and  $\delta$  are both taken as 10°;  $\lambda_1$  and  $\lambda_2$  are taken as 0.95 and 0.3, and calculated by substituting them into the numerical values Eq. (11).

$$\begin{cases} 95 \leq n_1 \leq 350 \\ 195 \leq n_2 \leq 500 \end{cases} \quad (11)$$

The teeth tip speed of the roller crusher is usually in the range of 0.5–3 m s<sup>-1</sup> (Shen et al., 2022). In the preliminary test, the teeth tip speed is required for efficient crushing when the upper roller teeth speed is between 100 and 300 r·min<sup>-1</sup>. At the same time, in order to achieve the interlocking shearing of the two roller teeth and form a tearing-squeezing composite effect, the lower crushing roller speed is designed to be 200–400 r·min<sup>-1</sup>.

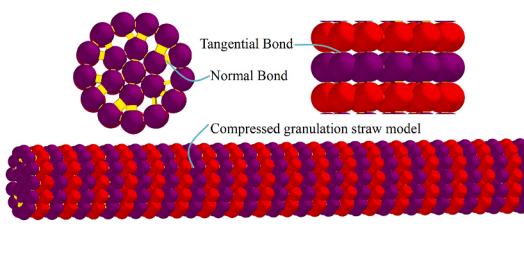
### 2.3. Construction of granulated straw group model

To clarify the mechanical properties of granulated straw and accurately build its simulation model, uniaxial compression tests were conducted using a universal material testing machine (RGM-4005). The normal deformation force of the material was analysed, while the tangential deformation force was examined through three-point bending and shear tests. The straw modeling method involved utilising different types of element particles to overlay the various types of straw particles in the cross-sectional unit, arranged both in parallel and staggered along the axial direction. These particles were connected through tangential and regular bonds to create a bidirectional anisotropic compression model of granulated straw (Fig. 5a). The length of the straw model was based on the actual distribution: 5–10 cm segments accounted for 38.7 %, 4–5 cm segments for 29.4 %, and crushed straw segments measuring 0–4 cm for 31.9 %.

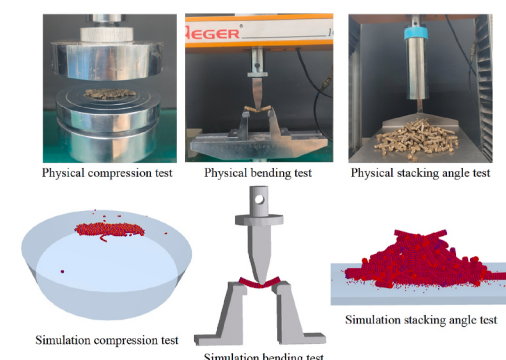
During the calibration tests, the fixture's moving speed was set to 20 mm min<sup>-1</sup>, and each test was repeated three times. A Box-Behnken (BB) test design was employed, utilising uniaxial compression and three-point bending tests to calibrate the normal and tangential bond parameters of the granulated straw. The elemental particle radius of granulated straw is 0.69 mm, and the Rayleigh time step of the calibration process is 1.85e-07 s. The inner and outer straw cross-sections contained 7 and 13 particles. The bond contact radius was fixed at 1.2 times the physical radius. The specific gravity of the tangential bond and the normal bond in the straw model is 1:3, and the tangential bond is more prone to fracture under stress during the crushing process. Additionally, the cylinder lifting test was used to calibrate the contact parameters (Fig. 5b). The bond parameters for the granulated straw referenced in this paper are presented in Table 1, while the contact parameters are outlined in Table 2.

**Table 1**  
Normal and tangential straw bond parameters.

Parameter	A/the normal stiffness per unit area and shear stiffness per unit area values of the normal bond	B/the normal strength and shear strength values of the normal bond	C/the normal stiffness per unit area and shear stiffness per unit area values of the tangential bond	D/the normal strength and shear strength values of the tangential bond	E/bond radius
Value	$5.59 \times 10^9$	$5.13 \times 10^6$	$3.42 \times 10^9$	$6.58 \times 10^7$	0.83



(a) Granulated straw model



(b) Calibration process of model

**Fig. 5.** Composition of granulated straw model.

**Table 2**  
Contact parameters of granulated straw.

Parameter	Value
Straw particle restitution coefficient	0.58
Straw particle static friction coefficient	0.72
Straw particle rolling friction coefficient	0.31
Straw particle and steel rolling restitution coefficient	0.68
Straw particle and steel rolling static friction coefficient	0.56
Straw particle and steel rolling friction coefficient	0.34

#### 2.4. Simulation test of single factor broken strip application

The discrete element simulation software was utilised to analyse the straw-crushing capacity of a differential counter roller. This study examined how the device's operating parameters influenced the crushing rate and defined the range of each influencing factor. The upper crushing roll, lower crushing roll, and ditching strip shovel were assembled using SolidWorks 2020 and imported into EDEM 2021.2 for simulation. It was employed to simulate and analyse the crushing process involving the upper and lower crushing rolls acting on granulated straw. During the simulation tests, the rotation speeds of both the upper and lower rollers, as well as the flow rate of the granulated straw, were considered as test factors. The number of broken bonds between straw particles was simulated to represent the crushing effect. The crushing rate of the granulated straw was defined as the ratio of the number of broken bonds to the total number of tangential bonds present (Chen et al., 2023). The total force of the bonds simulated the force applied by the rollers during the straw-crushing process.

The simulation was set to run for a duration of 1.5 s, with a Rayleigh time step of 6.5e-07 s. The simulation model is displayed in Fig. 6a. The height of the particle workshop was fixed at 250 mm, while the radius of the particles was varied at 60 mm, 70 mm, 80 mm, 90 mm, and 100 mm. The average particle flow rates in the workshop were recorded at 0.77 kg s<sup>-1</sup>, 0.99 kg s<sup>-1</sup>, 1.26 kg s<sup>-1</sup>, 1.49 kg s<sup>-1</sup>, and 1.77 kg s<sup>-1</sup> (Fig. 6b). Based on the theoretical analysis results in section 2.2.4 and existing crusher's operational parameters, the rotation speed range for the upper crushing roll was determined to be between 100 and 300 r·min<sup>-1</sup>, while the lower crushing roll's rotation speed ranged from 200 to 400 r·min<sup>-1</sup>. The test scheme is detailed in Table 3.

#### 2.5. Construction of interaction model between device-soil-flexible straw

Without reliable theoretical analysis, discrete element modelling and analysis of the mechanised strip application process can accurately predict and analyse the operation quality in the process. This is

**Table 3**

Single factor test of working parameters of straw crushing strip application device.

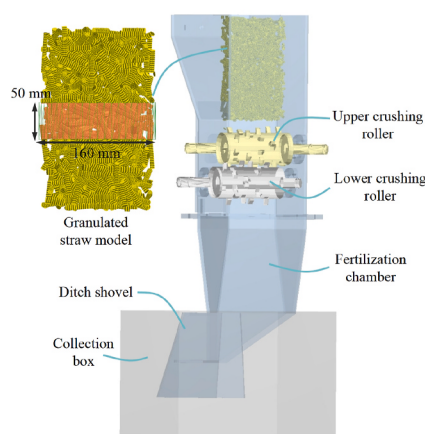
Test No.	Working parameters of strip applicator		
	Particle factory radius/mm	Upper crushing roller speed/r·min <sup>-1</sup>	Lower crushing roller speed/r·min <sup>-1</sup>
1	60,70,80,90,100	200	300
2	80	100,150,200,250,300	300
3	80	200	200,250,300,350,400

significant in reducing the number of field trials, costs, and efficiency of strip applications (Gong et al., 2022). The modelling in the paper involves the interaction between device-soil-flexible straw.

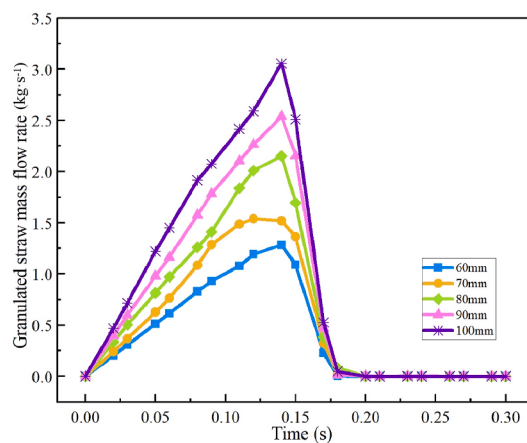
#### 2.5.1. Device-soil-flexible straw interaction model

The application process involves the crushing of flexible straw, mechanical trenching, soil covering, and compaction. Compared with traditional rigid material modelling, the coupled model can simulate the crushing and conveying relationship between the flexible body of granulated straw and the roller crushing device. The traditional rigid straw modelling method can only simulate the behaviour of a single straw cleaning and conveying process. The entire process of straw crushing, strip application, trenching, and deep straw burial involves the interaction between flexible straw, roller device, and soil particles, and the model construction is relatively complex. The model constructed can simulate the force crushing of flexible straw, the interaction between the trenching shovel, compaction wheel, and covering disc and soil particles during the trenching process of the strip application device, as well as the distribution of straw in soil particles after crushing.

The soil used in the granulated straw strip application test is humic gley soil, which is based on loam soil and has a high proportion of sand and silt particles. The overall state is mainly composed of loose particle stacking. During the strip application process, the soil layer is broken by a vertical soil crushing device, and the bonding characteristics between soil particles are reduced. The Hertz-Mindlin (no ship) contact model was selected to establish a soil trough with length × width × height (1100 mm × 600 mm × 240 mm). The contact parameters between soil particles are shown in Table 4. The straw crushing strip application device, soil covering disc, and compaction wheel model were introduced into the soil trough to build a simulation model of mechanised strip application of granulated straw (Fig. 7). During the process of straw crushing and strip application, the fixed time step of the simulation is 20 %, Rayleigh time step is 3.71e-07 s, target save interval



(a) Single factor simulation test model



(b) Particle flow in the particle factory

Fig. 6. Compression granulated straw model.

**Table 4**

Parameter setting for discrete element simulation of mechanised strip application.

Parameter	Numerical value
Poisson's ratio of soil particles	0.40
Poisson's ratio of straw particles	0.25
65 Mn steel Poisson's ratio	0.35
Shear modulus of soil particles/Pa	$1 \times 10^6$
Shear modulus of straw particles/Pa	$1 \times 10^8$
65 Mn steel shear modulus/Pa	$7.27 \times 10^{10}$
Recovery coefficient between soil particles	0.20
Dynamic friction coefficient between soil particles	0.30
Static friction coefficient between soil particles	0.40
Recovery coefficient between soil particles and straw	0.50
Dynamic friction coefficient between soil particles and straw	0.01
Static friction coefficient between soil particles and straw	0.50
Recovery coefficient between soil particles and 65Mn steel	0.30
Dynamic friction coefficient between soil particles and 65Mn steel	0.05
Static friction coefficient between soil particles and 65Mn steel	0.50

is 0.01 s and soil particle radius is 5 mm. The structure of the strip application device is a circular disc with overburden angle of 20°, a diameter of 406 mm, and a digging shovel tip inclination angle of 73°.

Based on the above single factor simulation analysis, the rotation speed of the upper and lower rollers of the strip application device has an important impact on the straw crushing rate and the uniformity of strip application. It is preferred that the rotation speed of the upper roller is 100–200 r·min<sup>-1</sup>, and the rotation speed of the lower roller is 300–400 r·min<sup>-1</sup>. Combined with the forward speed and ditching depth in the actual operation process of the device, it has an important impact on the uniformity of strip application of straw. The operation speed should not be too fast because the machines need to be used for trenching and strip application. Select the forward speed of the machines as 3–5 km h<sup>-1</sup>, the depth of trenching and strip application as 100–200 mm, and design the L<sub>9</sub> (3<sup>4</sup>) uniform design test table to carry out the uniform design test of four factors and three levels.

#### 2.5.2. Orthogonal test and evaluation index

In the process of mechanised strip application of granulated straw, the crushing rate and uniformity determine the test quality, which will affect the subsequent growth of crops and then affect the crop yield. Therefore, the straw crushing rate and the coefficient of variation of strip application were selected as the evaluation indexes of the simulation test. The variation coefficient of strip uniformity refers to DB/T106-

2019 fertiliser spreader test standard. Three mass sensors (length × width × height: 100 mm × 200 mm × 100 mm) are set in the forward direction of the strip applicator. By calculating the straw mass  $M_i$  in each sensor, the variation coefficient of strip uniformity  $Y_a$  is obtained as Eq. (12).

$$Y_a = \frac{\sqrt{\frac{1}{3-1} \sum_{i=1}^3 (M_i - \bar{M}_1)^2}}{\bar{M}} \times 100\% \quad (12)$$

where  $M_1$  —  $\bar{M}_1$  is the average mass of the three sensors for straw strip application, kg.

#### 2.6. Validation and analysis of device operation parameters

To verify the accuracy of the operation parameters for the straw-crushing strip application device, which was optimised through simulation tests, a field test was conducted in November 2023. The test took place at the Ningyue Agricultural Machinery Company's site in Heishan County, Liaoning Province, China (coordinates: 41.671°N, 122.131°E). According to the classification criteria of World Reference Base (WRB) for Soil Resources, the soil at the test site is classified as humic gleysoil. The straw treatment involves crushing, covering, and returning the straw to the field during the maize harvest, using the crushing mechanism of the combine harvester. After the straw is crushed, a straw granulator collects and compresses it into granules. Following this process, there is no remaining straw on the ground, only maize stubble. The strip applicator operates between the maize rows to avoid contact with the stubble (Fig. 8).

The main test instruments are Luoyang Ruide RM2004 tractor, SC900 cone-index soil compactometer, shovel, calliper, φ50.46 mm × 50 mm soil sampling ring knife, drying oven, electronic balance (accuracy 0.01 g). When selecting soil samples, according to the standards GB/T 36197-2018 and NY/T 1121, soil samples are taken along an S-shaped route in rectangular terrain according to the principles of random, equal, and multi-point mixing. The straight-line distance between adjacent sampling points is greater than 10 m, and the distance between sampling points and the edge of the field is greater than 15 m. Use the compactometer to measure the soil compactness of 0–300 mm, use the soil ring knife to take soil and weigh it by balance, and finally, dry it in the oven to calculate the soil moisture content and bulk density. Other soil characteristic parameters within 0–300 mm of the soil layer are shown in Table 5.

During test, the output speed of the hydraulic motor is controlled by

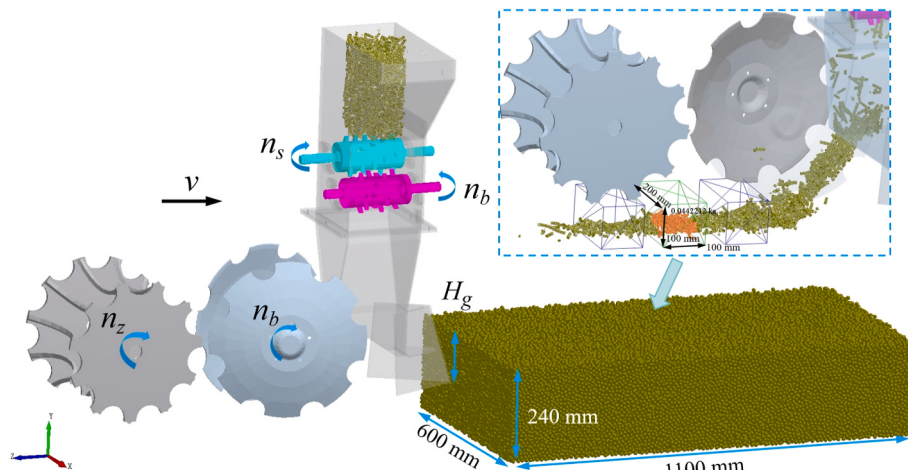


**Fig. 7.** Simulation model of mechanised strip application of granulated straw

Note:  $n_z$  is the speed of the pressing wheel, r·min<sup>-1</sup>;  $n_b$  is the speed of disc, r·min<sup>-1</sup>;  $H_g$  is the straw strip application depth, mm;  $v$  is the forward speed, km·h<sup>-1</sup>; The volume of soil bin is length × width × height (1100 mm × 600 mm × 240 mm).

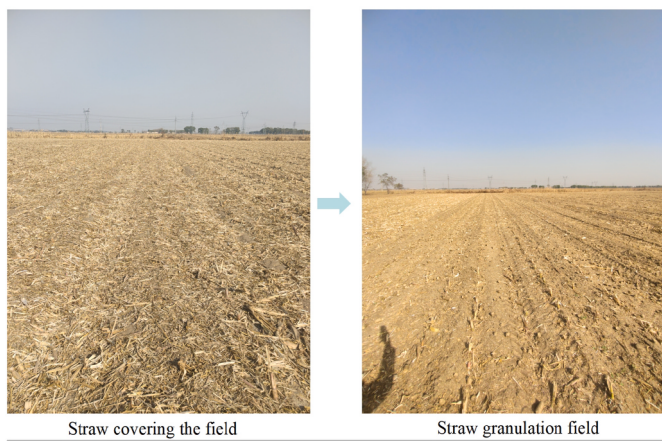


**Fig. 8.** Surface conditions during field tests.

the speed-regulating valve, and the speed of the crushing roller is regulated to the optimal range. Adjust the height of the profiling wheel from the ground so that the depth of the trenching shovel is fixed at 150 mm, and the tractor operating speed is controlled at about 5 km h<sup>-1</sup> (Fig. 9). Since the surface soil of no-tillage in Northeast China is relatively complex and the direct penetration resistance of the trenching shovel is significant, a vertical soil-breaking device is installed in front of the trenching shovel, which will stir up the hard soil blocks on the surface during operation, to avoid large soil blocks in the process of strip application and affect the quality of strip application. In section 2.5, the Hertz-Mindlin (no slip) model suitable for loose soil is used to carry out the simulation test. The vertical soil crushing device will crush the hard soil, and the working condition of the trenching shovel is closer to the simulation test process (Chen et al., 2024). The straw at the sampling points was weighed with an electronic balance to measure the 0–4 cm straw mass proportion, and the straw crushing rate was calculated by combining the original granulated straw length proportion. The coefficient of variation  $Y_b$  of uniformity of straws is Eq. (13).

$$Y_b = \sqrt{\frac{\frac{1}{10-1} \sum_{i=1}^{10} (M_i - \bar{M}_2)^2}{\bar{M}}} \quad (13)$$

where  $M_2$  is the average mass in ten lengths (200 mm × 200 mm) of the discharge area, kg.

### 3. Results and discussion

#### 3.1. Single factor test results of straw crushing strip application

During the simulation test, the straw was in contact with the upper crushing roll at 0.1–0.2 s and was diverted to the lower crushing roll. At 0.2–0.9 s, the straw begins to be broken under the action of the differential rollers. Many straws are sheared and broken under the action of the differential rollers and discharged from the teeth of the two rollers. The straw is broken from long to short particles, which is convenient for rapid decay in the subsequent mechanised strip application process. At 0.9–1.5 s, the straw is crushed and discharged from under the ditching shovel under the action of gravity (Fig. 10).

**Table 5**  
Soil characteristic parameters.

Depth/mm	Soil bulk density/g·cm <sup>-3</sup>	Compactness/kPa	Moisture content/%
0–100	1.32	935	9.4
100–200	1.45	1567	13.4
200–300	1.71	2639	16.7

#### 3.1.1. Effect of straw flow change on straw fracture and bond force

It is determined that the speeds of the upper and lower rollers are 200 r·min<sup>-1</sup> and 300 r·min<sup>-1</sup>, and the particle factory radius is 60, 70, 80, 90, and 100 mm, respectively (Fig. 11).

The test results showed a fluctuating trend with the increase in the flow rate of granulated straw, the broken rate, and the force fracture of straw. When the particle flow rates were 0.77 kg s<sup>-1</sup>, 0.99 kg s<sup>-1</sup>, 1.26 kg s<sup>-1</sup>, 1.49 kg s<sup>-1</sup> and 1.77 kg s<sup>-1</sup>, the straw crushing rates were 21.6 %, 19.4 %, 19.9 %, 20.4 % and 21.7 %, respectively. The straw crushing rate increased slightly with the increase in particle flow rate. Except for the small particle flow rate of 0.77 kg s<sup>-1</sup>, the change of straw crushing rate with the change of flow rate was small and maintained at about 5.0 %. The above analysis indicates that appropriately increasing the flow rate of straw can help improve the breakage rate of straw, which may be directly related to the formation of particle clusters due to the large amount of straw, which accumulate at the side wall position and reduce the amount of straw flowing out from the side wall.

The force fracture of the bond in the range of 60–70 mm shows that the total force of bond fracture is greater than 70 mm when the particle factory radius is 60 mm. In the range of 80–100 mm, the bond fracture force increases with the increase of flow rate. At stage I of 0–0.2 s, the bond began to break, and the force on the straw bond increased rapidly. The counter roll device contacted the straw particles and began to break the straw. At stage II of 0.2–0.8 s, the number of broken straws increased continuously, and the force of broken straw bonds increased rapidly. Stage III of 0.8–1.5 s is at the end of the crushing stage. At this time, bond fracture does not occur, and the force of bond fracture remains stable and does not increase.

Comparing the straw crushing conditions under different flow rates, the straw crushing rate has an increasing trend with the increase of straw flow rate, which may be due to the increase in contact times between straws, making the straw more prone to crushing. In Fig. 12a–j, the process of straw crushing has gradually increased with the increase of straw flow rate.

The results indicate that within the granulated straw flow rate range of 0.77–1.77 kg s<sup>-1</sup>, the straw crushing rate remains relatively stable, fluctuating by only about 5.0 %. This confirms the appropriateness of the chosen roller teeth structure parameters and installation settings. Under varying flow conditions, the crushing effect of the straw and the resulting stacking angle stabilise within the range of 0.99–1.26 kg s<sup>-1</sup> (Fig. 13). However, when the flow rate increases to between 1.49 kg s<sup>-1</sup> and 1.77 kg s<sup>-1</sup>, the stacking angle of the granulated straw rises due to the limited volume of the box.

#### 3.1.2. Effect of upper crushing roller speed on straw fracture and bond force

It is determined that the particle factory radius is 80 mm, the rotation speed of the lower roller is 300 r·min<sup>-1</sup>, and the rotation speed of the upper roller is 100, 150, 200, 250, 300 r·min<sup>-1</sup> (Fig. 14).

The test results showed that with the increase of the rotation speed of the upper roller, the straw crushing rate and the force fracture situation showed a fluctuating trend, and the straw crushing rates were 20.4 %, 18.0 %, 19.2 %, 18.6 %, 21.2 %, respectively. In the range of 100–200 r·min<sup>-1</sup>, with the increase of rotation speed, the straw crushing rate first decreased and then increased, and in the range of 200–300 r·min<sup>-1</sup>, the straw crushing rate also showed a trend of decreasing first and then increasing. The straw crushing rate is the same in the two ranges. The total force of bond breaking is more minor in the range of 100–200 r·min<sup>-1</sup>, and the total force of straw breaking is 1008 N, 991 N, 1019 N in 1.5 s, and 1042 N, 1091 N in the range of 250–300 r·min<sup>-1</sup>, respectively. Therefore, in the range of smaller rotating speeds, it is helpful to reduce the torque of the crushing roller during operation. At stage I of 0–0.2 s, the straw bond began to break. At this time, the number of broken bonds began to differ with the rotation speed of the upper roller. At stage I, the force of bond fracture increased rapidly, and the straw began to be broken. At stage II of 0.2–0.8 s, the number of broken straws and the total force of broken straw bonds increased rapidly. At Stage III



**Fig. 9.** Test device for straw crushing strip application.

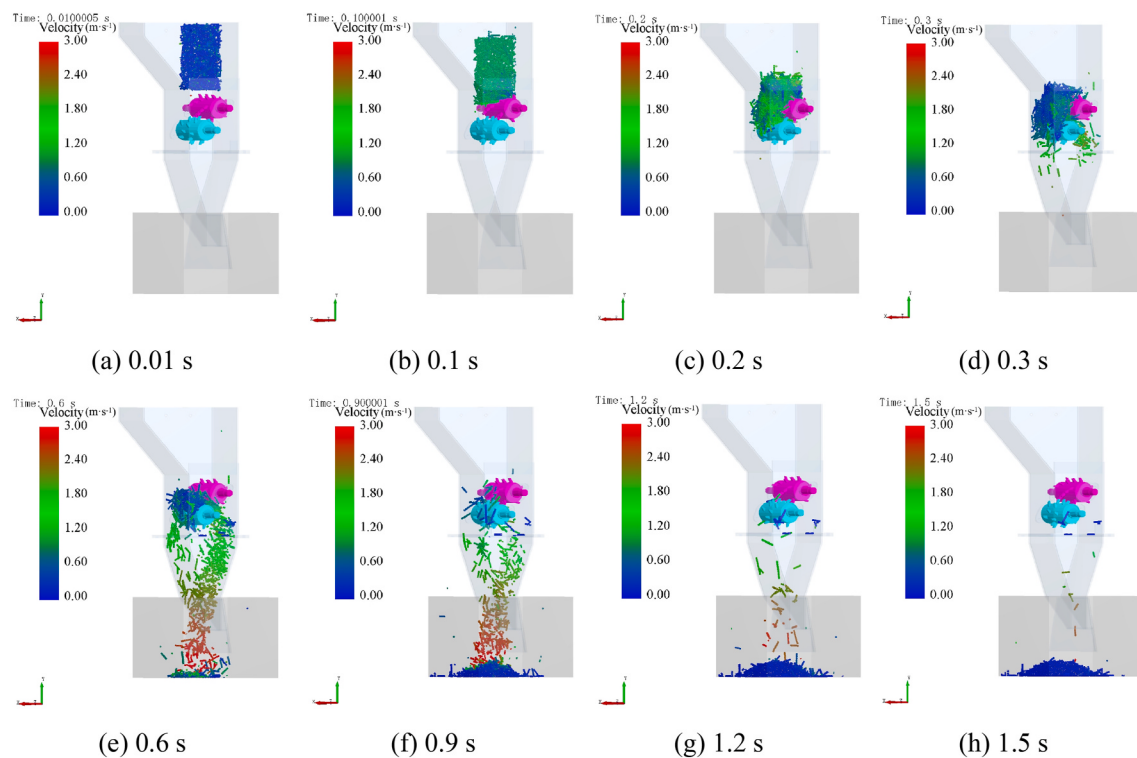


**Fig. 10.** Process of simulation test of straw crushing (the speed of upper crushing roll is  $200 \text{ r} \cdot \text{min}^{-1}$ , the speed of lower crushing roll is  $300 \text{ r} \cdot \text{min}^{-1}$ , and the radius of particle factory is 80 mm).

of 0.8–1.5 s, bond fracture does not occur, and the force of bond bond fracture remains stable and does not increase.

Comparing the straw crushing conditions under different upper roller speeds, the straw crushing rate fluctuated with the increase in the upper roller speed. The upper roller can first contact the straw group and play the role of diversion. When the upper roller speed is too high, some straw will be thrown to the side wall of the shovel body, which will not be crushed by the extrusion of the roller and flow out of the side wall of the shovel body, thus reducing the straw crushing rate (Chen et al., 2021). At the same time, the upper roll's rotation speed will affect the opposite roll's differential speed ratio and then affect the straw crushing rate (Fig. 15).

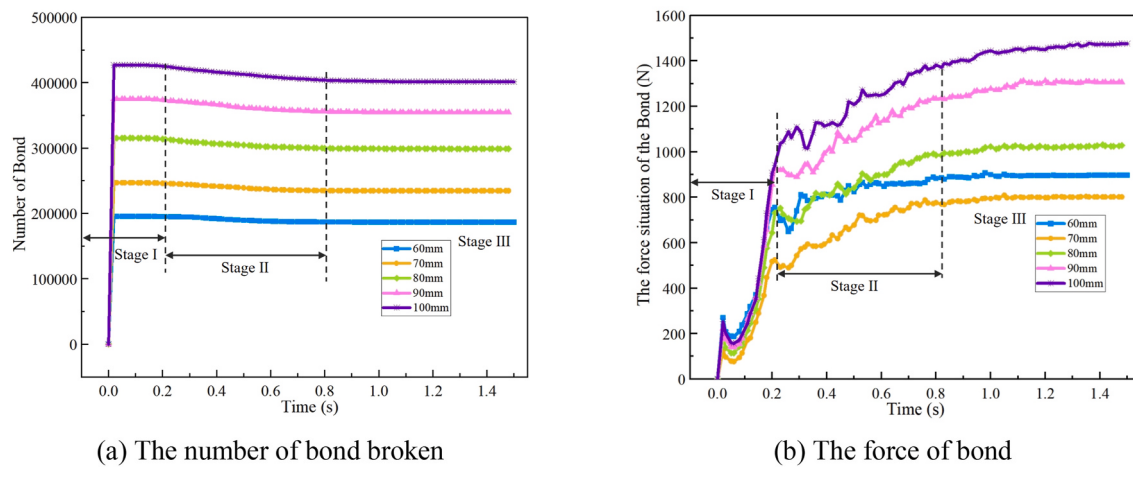
### 3.1.3. Effect of lower crushing roller speed on straw fracture and bond force

It is determined that the particle factory radius is 80 mm, the rotation speed of the upper roller is  $200 \text{ r} \cdot \text{min}^{-1}$ , and the rotation speed of the

lower roller is  $200, 250, 300, 350, 400 \text{ r} \cdot \text{min}^{-1}$  (Fig. 16).

The test results showed that with the increase of the rotation speed of the lower roller in the range of  $200\text{--}400 \text{ r} \cdot \text{min}^{-1}$ , the straw crushing rate and the total force of straw fracture showed an increasing trend. The straw crushing rates were 18.6 %, 19.0 %, 20.2 %, 19.2 %, and 20.7 %, respectively. The total force of straw fracture was 988 N, 1021 N, 1042 N, 1059 N, and 1055 N. The straw crushing rate was high in the  $300\text{--}400 \text{ r} \cdot \text{min}^{-1}$ , and the force increased slightly compared with  $250 \text{ r} \cdot \text{min}^{-1}$ . At stage I of 0–0.2 s, the straw bond began to break. At this time, the crushing rate differed with different rotation speeds of the lower roller. At stage II of 0.2–0.8 s, the straw is in the straw-crushing stage. With the increase of the rotation speed of the lower roller, the number of broken straws increases, and the total force of the broken straw bond increases. At stage III of 0.8–1.5 s, the bond fracture does not occur, and the force of bond fracture does not increase, keeping it stable.

With the increase of the speed of the lower roller, the shear crushing



(a) The number of bond broken

(b) The force of bond

Fig. 11. Effect of straw flow change on straw fracture and bond force.

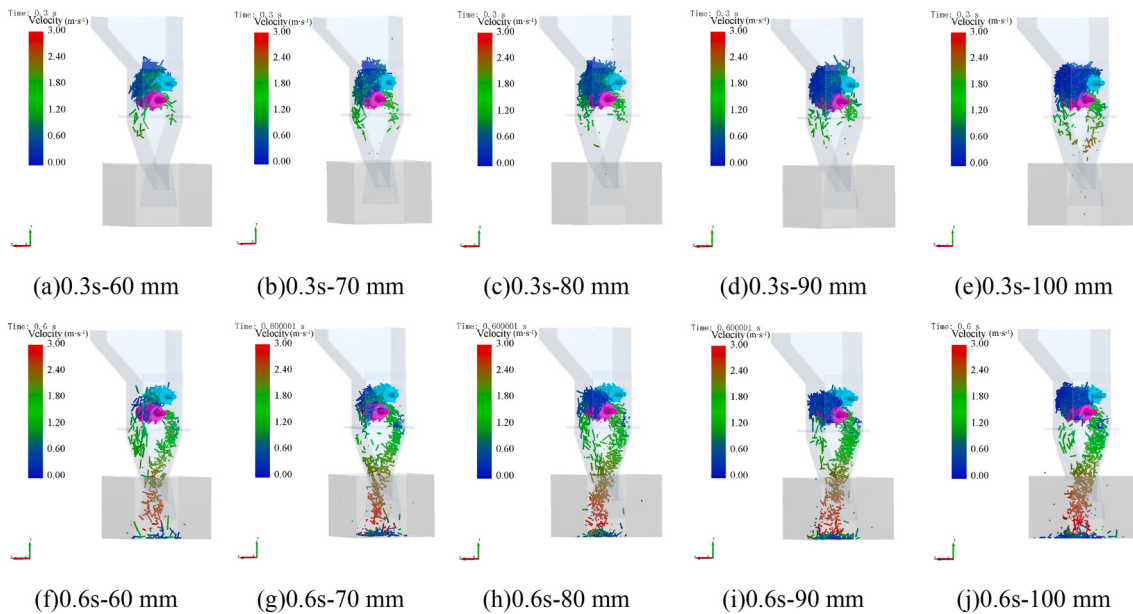


Fig. 12. Effect of flow change on straw breaking strip application.

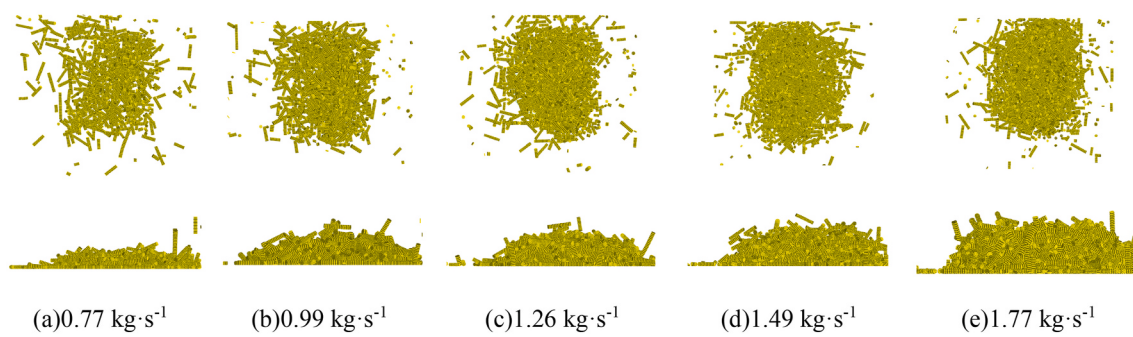
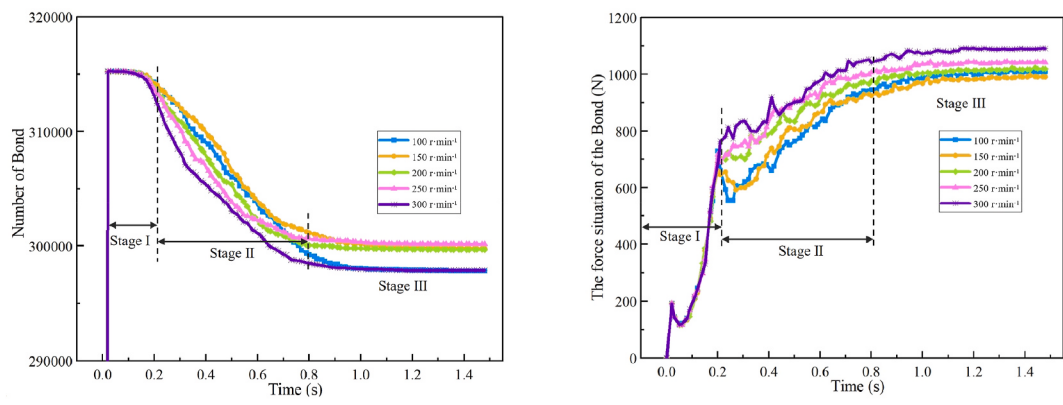


Fig. 13. Crushing effect and formed stacking angle of straw under different flow conditions.

of straw was enhanced, and the straw crushing rate showed an increasing trend (Fig. 17). The increase of the rotation speed of the lower roller will prevent the straw from contacting with the side wall of the shovel, reduce the number of straws falling along the side wall, and promote the crushing of straws through the extrusion of the roller, thus

increasing the straw crushing rate (Chen et al., 2021).

In conclusion, there was little difference in the change of straw crushing rate with flow rate in the range of 0.77–1.77 kg s<sup>-1</sup>. Therefore, the differential speed has little influence on the flow change during the operation of the roller straw-crushing device. When the upper roller's



(a) The number of bond broken

(b) The force of bond

Fig. 14. Analysis of upper roller speed on straw fracture and bond force.

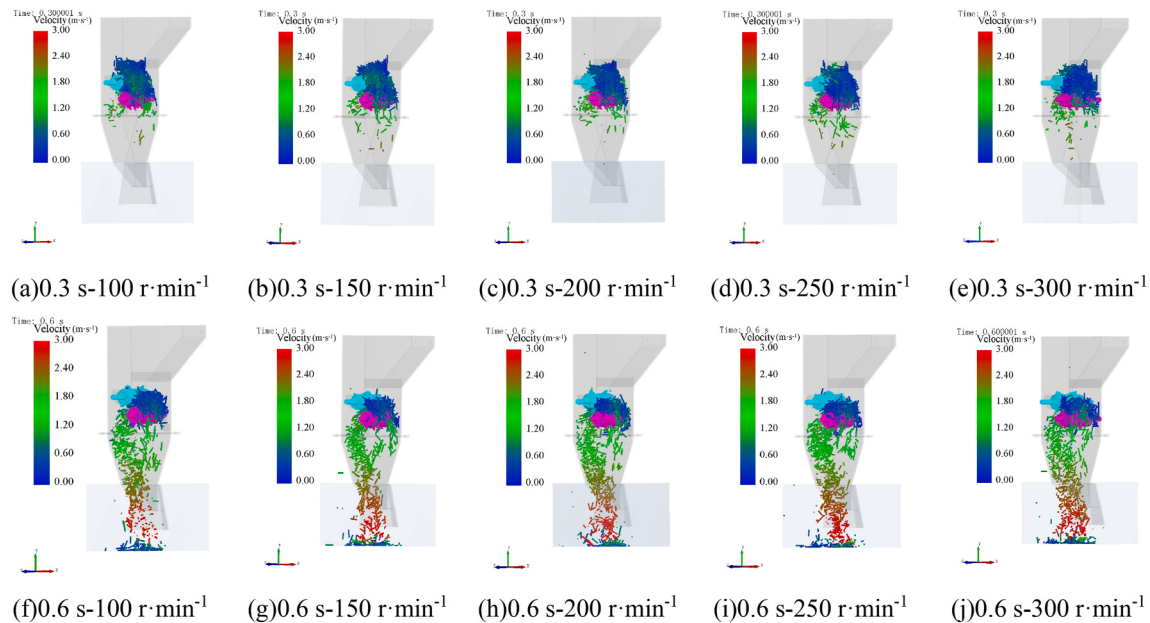
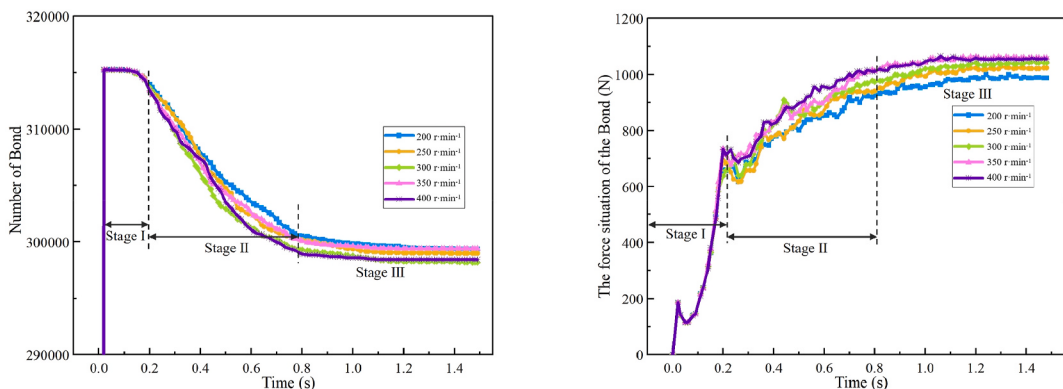


Fig. 15. Analysis of speed change of upper roller on straw crushing strip application.



(a) The number of bond broken

(b) The force of bond

Fig. 16. Analysis of lower roller speed on straw fracture and bond force.

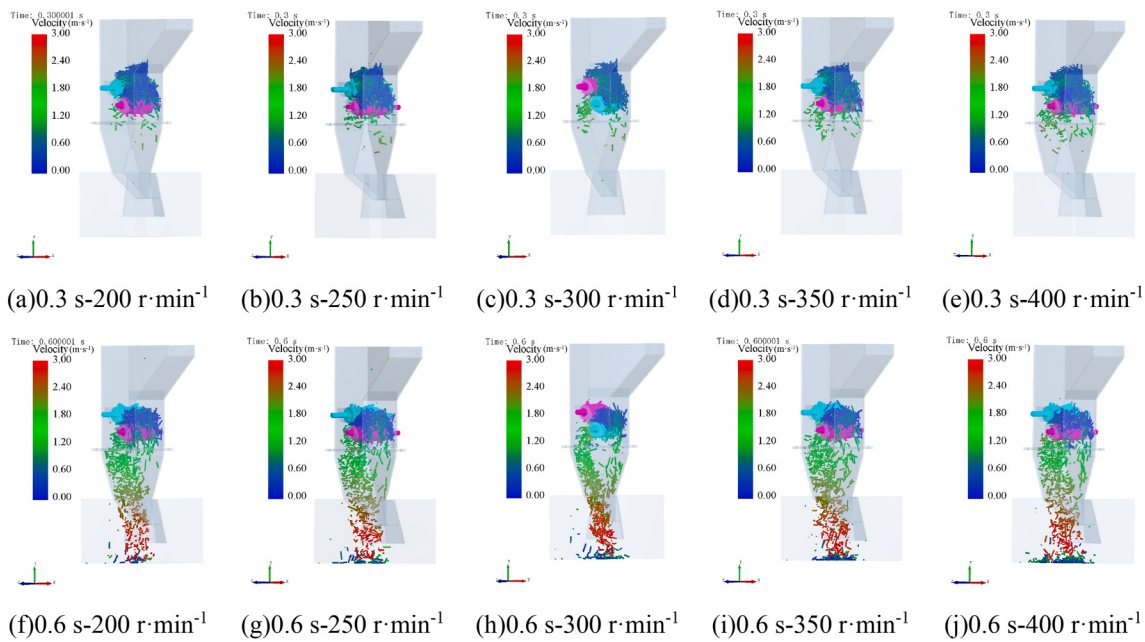


**Fig. 17.** Analysis of the speed change of the lower roller on the straw crushing strip application.

speed is  $100\text{--}200\text{ r}\cdot\text{min}^{-1}$ , the straw crushing rate is higher, the straw crushing rate decreases first and then increases, and the force of the device is smaller. The straw crushing rate was high in the range of  $300\text{--}400\text{ r}\cdot\text{min}^{-1}$  for the rotation speed of the lower roller. The single-factor test confirmed the influence of the straw flow and the rotation speed of the upper and lower rollers on the straw crushing rate and optimised the parameter selection range. The research process can provide corresponding technical references for optimising the roller device to crush fertiliser, coal, soil, harvest pepper, process walnuts, and

aquatic products (Fang et al., 2022; Gong et al., 2022; Sun et al., 2024).

### 3.1.4. The mechanism of straw crushing and strip application

Granulated straw relies on gravity to fall into the crushing zone where the roller is located. As the roller teeth rotate, they create disturbances that accelerate the movement of the straw (Fig. 18a). The granulated straw is crushed by the shearing and squeezing action of the roller teeth, which then expels the crushed material through a gap in the reserved area on the teeth side (Fig. 18b and c). Once the crushing

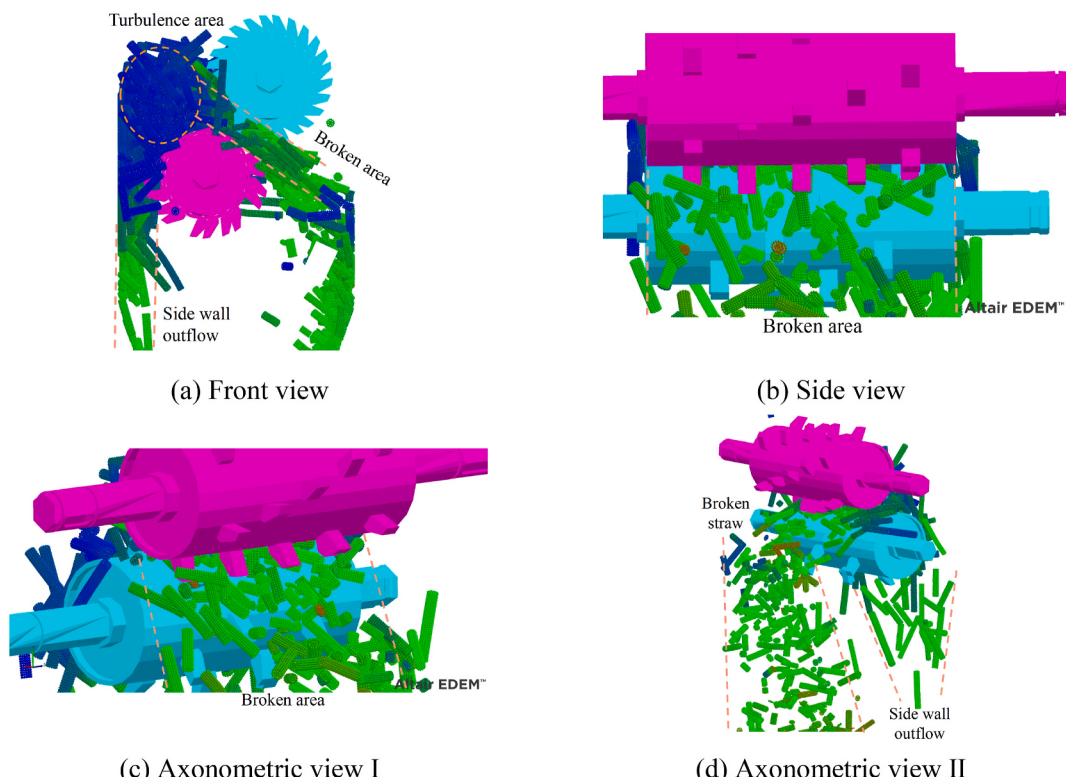


**Fig. 18.** Process diagram of straw crushing by differential granulation with rollers.

process is complete, the roller teeth disengage from the meshing position and stop crushing the granulated straw. The crushed particles are then discharged through the strip application port, relying on their own gravity (Fig. 18d).

### 3.2. Simulation analysis of mechanised strip application process

#### 3.2.1. Test scheme and results

A uniform design test table [ $L_9(3^4)$ ] was developed to carry out the test of four factors and three levels. The test scheme is shown in Table 6. The analysis of strip application simulation test results is shown in Table 7. Orthogonal tests can be used to analyse the effects of different groups on the crushing rate and variation coefficient of uniformity of granulated straw during strip application. The optimal operating parameters of the strip application device can be optimised, providing a basis for designing the device structure and operating parameters.

#### 3.2.2. Analysis of simulation test results of strip application

As shown in Fig. 19, in the mechanised strip application of granulated straw, the trenching shovel, covering disc, and compaction wheel cooperate to complete the strip application of granulated straw. The test process is divided into three stages: I. The trenching shovel pushes the soil particles in the soil bin forward and upward and turns the soil particles at the depth of trenching up along the side of the shovel tip. II. The straw slide down along the cavity after being extruded and rubbed by two crushing rollers and finally fall into the ditch opened by the ditching shovel. III. The passive rotation of the covering disc causes the soil particles overturned by the ditching device to move to the ditch through the inner side of the disc and complete the soil covering. The inclination of the disc can adjust the amount of soil covering, and the wheel rotates passively to compact the soil covering layer.

Comparative analysis was carried out in groups 1, 2, and 3 of the test. At the initial time of soil penetration (0.25 s), Fig. 19a–c, when the trenching shovel tip enters the soil groove, the soil particles tend to rise upward, and the movement speed of soil particles is the largest at the position perpendicular to the shovel tip plane and the contact position of the shovel tip. With the increase of operation speed and strip depth, the movement speed of soil surface particles and the range of soil disturbance increased (Barr et al., 2020). The movement speed of soil particles and the disturbed area of soil particles are positively correlated with the operation speed and strip depth (Wang et al., 2019). However, in the actual process of ditching, the greater the disturbance of the shovel tip on the soil surface, the greater the evaporation of soil moisture, which is not conducive to the protection of soil moisture, so it is necessary to reduce the disturbance of the shovel tip on the soil surface (Aikins, Ucgul, et al., 2021; Hang et al., 2017). Excessive speed of the shovel tip can easily throw soil particles towards both sides of the ditch, resulting in a poor soil return effect of the disc covering the soil.

At the time of stable strip application (0.5–0.75 s), Fig. 19d–i, the ditching shovel realises stable ditching operation, the two rollers cooperate to realise the crushing strip application of granulated straw, and the stable crushing strip application of granulated straw is realised under the interaction of roller, ditching shovel and disc. With increased strip application depth, soil blocking appeared above the ditching shovel (Fig. 19f–i). Under the condition of no-tillage, the disturbance to the

**Table 6**

Various factors in the orthogonal simulation process of granulated straw strip application.

Levels	Upper roller speed $n_s$ ( $r \cdot min^{-1}$ )	Lower roller speed $n_x$ ( $r \cdot min^{-1}$ )	Strip depth $H_g$ (mm)	Forward speed $v$ ( $km \cdot h^{-1}$ )
1	100	300	100	3
2	150	350	150	4
3	200	400	200	5

**Table 7**

Orthogonal test scheme and results of granulated straw strip application.

Test No.	$n_s$ ( $r \cdot min^{-1}$ )	$n_x$ ( $r \cdot min^{-1}$ )	$H_g$ (mm)	$v$ ( $km \cdot h^{-1}$ )	Crushing rate (%)	Variation coefficient of uniformity (%)
1	100	300	100	3	33.4	17.7
2	100	350	150	4	35.5	15.0
3	100	400	200	5	31.5	16.5
4	150	300	150	5	42.0	14.4
5	150	350	200	3	47.2	18.8
6	150	400	100	4	28.2	20.8
7	200	300	200	4	51.0	15.6
8	200	350	100	5	28.4	16.8
9	200	400	150	3	41.1	22.3

surface soil should be reduced as much as possible to avoid soil blocking (Chen et al., 2024; Hou et al., 2022).

At the end time of strip application (1.0 s), as shown in Fig. 19j–l, the granulated straw is strip applied to the soil. As shown in Fig. 19j–k, the covering disc will affect the straw particles buried on the surface layer during the operation, affect the burial depth of the strip-applied straw, and have a particular impact on the uniformity distribution of the strip-applied straw. Therefore, in the process of mechanised strip application, the depth of the disc should be adjusted according to the strip application depth to improve the uniformity of strip application.

#### 3.2.3. Force analysis of strip application process device

Select the time (1.2 s, 1.0 s, 0.8 s) when the trenching shovel is in the middle of the soil trough in the 1, 2, and 3 groups of tests to analyse the force of the strip application device (Fig. 20). The results showed that the force of the contact part between the strip application device and the soil during the operation was mainly concentrated in the tip part of the trenching shovel. With the increase of the operation depth and forward speed, the force at the tip increased, and the force at the side edge of the covering disc and the compaction wheel increased. This will increase the wear of the shovel tip, so the manufacturing of shovel tips requires materials with high strength and good wear resistance. The total force values of the trenching shovel three times are 256.4 N, 744.9 N, and 2550.4 N, respectively. With the increase of ditching depth, the force distribution above the shovel tip is large, and the soil will be loose when the strip depth is 200 mm, and the force will increase sharply. Therefore, the trench depth and the disc's covering soil should not be too large during the application process.

#### 3.2.4. Analysis of soil particle movement velocity and total force

During the process of trenching, covering soil, and compaction during the comparative operation, the movement speed of soil surface particles around the shovel tip during the application is much higher than that of other operation stages. The results show that under the same test conditions, the disturbance range of soil surface particles during the shovel tip trenching operation is the most extensive (Fig. 21).

The comparison of soil particle movement velocity at identical displacement positions reveals that as both operational speed and trenching depth increase, the disturbance range of the soil surface expands (Aikins, Ucgul, et al., 2021; Hang et al., 2018) (Fig. 21a,b,c). Throughout the trenching process, which includes digging, covering, and compacting soil, the movement velocity of soil particles and the disturbance area are positively correlated with the operational speed and trenching depth. During actual trenching, greater disturbance caused by the shovel tip on the soil surface leads to increased evaporation of soil moisture, which is detrimental to maintaining soil moisture levels. Therefore, it is essential to minimise the disturbance caused by the shovel tip on the soil surface (Wang et al., 2020). This study aims to explore the interaction between the digging shovel and soil particles under varying speeds and digging depths, as well as to analyse the

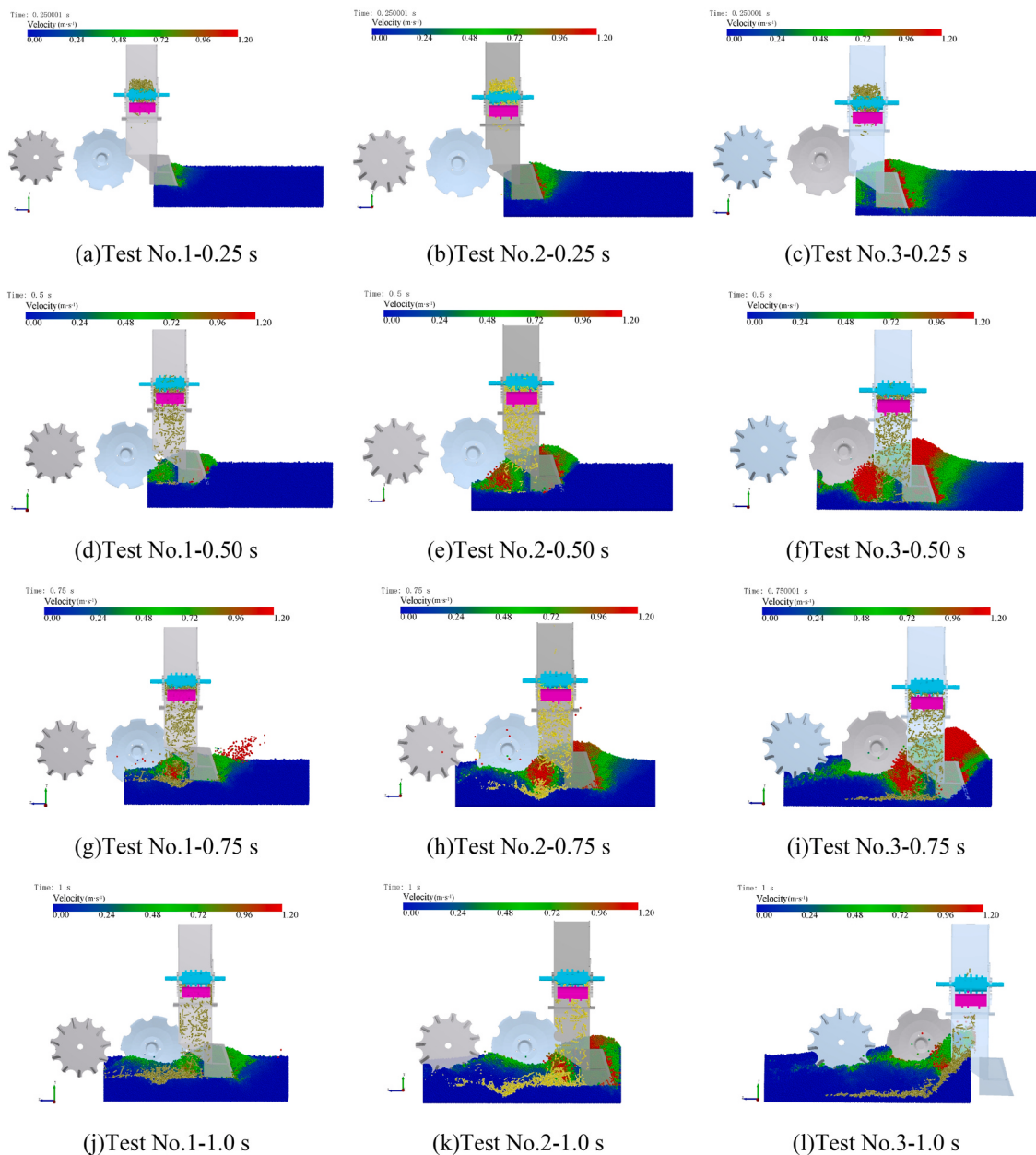


**Fig. 19.** Analysis of strip application process of granulated straw (Test No.1, 2, 3).

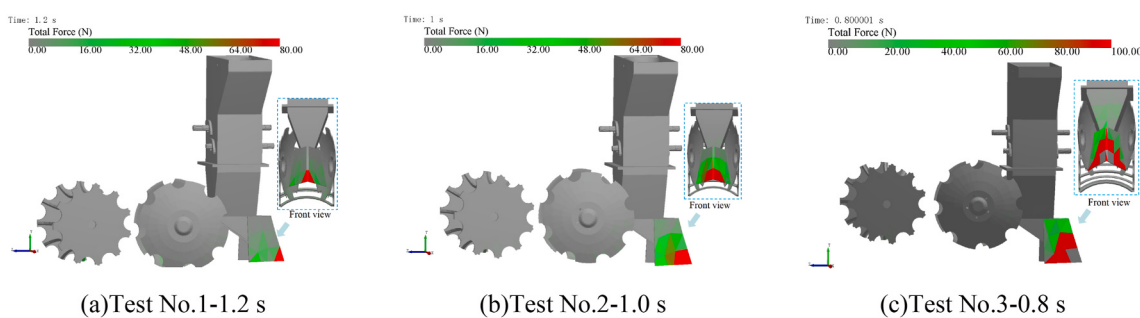


**Fig. 20.** Cloud chart of force analysis of strip device.

velocity of soil particles and the total force during the digging process.

The average soil particle velocity within 0–1.4 s of Test No. 1 ( $3 \text{ km h}^{-1}$ , 100 mm), Test No. 2 ( $4 \text{ km h}^{-1}$ , 150 mm), and Test No. 3 ( $5 \text{ km h}^{-1}$ ,

200 mm) is  $0.04 \text{ m s}^{-1}$ ,  $0.07 \text{ m s}^{-1}$ , and  $0.12 \text{ m s}^{-1}$ , respectively (Fig. 22a). The soil particle velocity increases with both the depth of the ditch and the advancing speed, with the most significant increase

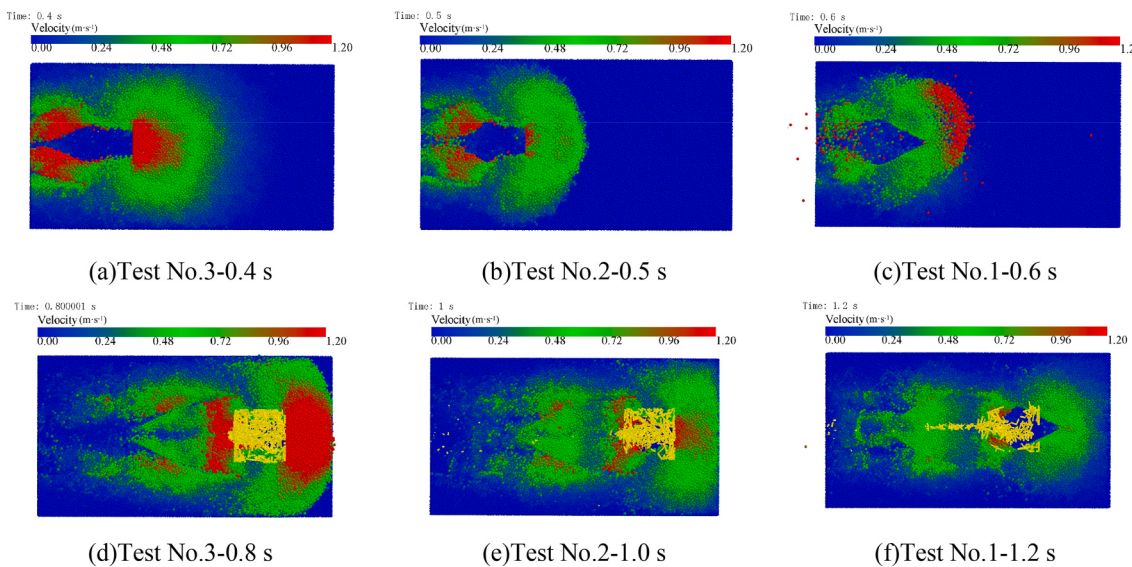


Fig. 21. Comparison of soil particle movement velocity.

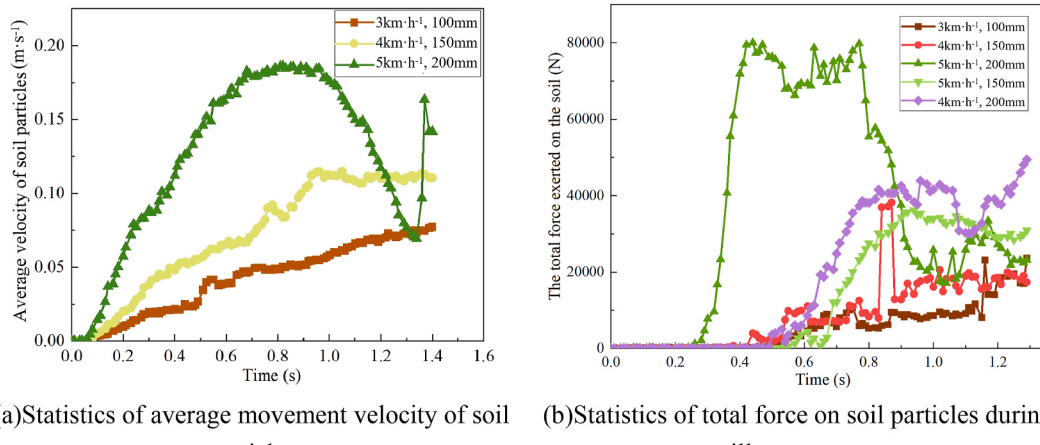


Fig. 22. Comparison of soil particle velocity and force analysis during strip application process.

observed in Test No. 3. The total force exerted on the soil particles within 0–1.4 s for Tests No. 1, 2, and 3 is 5648 N, 9006 N, and 36722 N (Fig. 22b). When controlling the test speed at 5 km h<sup>-1</sup>, the average total forces for Test No. 3 (5 km h<sup>-1</sup>, 200 mm) and Test No. 4 (5 km h<sup>-1</sup>, 150 mm) are 36722 N and 14193 N, respectively. By keeping the trench depth at 200 mm and comparing Test No. 3 (5 km h<sup>-1</sup>, 200 mm) with Test No. 7 (4 km h<sup>-1</sup>, 200 mm), the average total forces on the soil particles are 36722 N and 19338 N.

The results indicate that the operational speed has less impact on soil disturbance compared to the depth of the ditch. When the operational speed is set at 4 km h<sup>-1</sup>, there is a notable increase in both soil particle movement speed and total force on soil particles within the depth range of 150–200 mm as ditch depth increases, leading to greater disturbance of soil particles. Consequently, it is recommended that the ditch depth be maintained below 200 mm, with a final decision to set it at 150 mm.

### 3.2.5. Optimisation of plant operation parameters

Through the above simulation analysis, in order to achieve a better effect of strip application with higher straw crushing rate and uniformity variation coefficient of straw, it is necessary to optimise the operation parameters. As shown in Table 8, the analysis of variance shows that the model is significant and the regression equation has extremely

**Table 8**  
Variance analysis of test results of straw strip application process.

Project	Variation source	df	Sum of squares	Mean square	F	P
Crushing rate	Regression	4	504.58	126.146	16.27	0.010***
$n_s$	1	67.34	67.335	8.69	0.042**	
$n_x$	1	109.23	109.227	14.09	0.020**	
$H_g$	1	262.68	262.682	33.89	0.004***	
$v$	1	65.34	65.34	8.43	0.044**	
Error	4	31.01	7.751			
Total	8	535.59				
Uniformity coefficient of strip application	Regression	4	52.746	13.186	11.91	0.017**
$n_s$	1	4.932	4.932	4.45	0.102	
$n_x$	1	23.960	23.960	21.63	0.010**	
$H_g$	1	3.096	3.096	2.80	0.170	
$v$	1	20.758	20.758	18.74	0.012**	
Error	4	4.431	1.108			
Total	8	57.176				

Note: \*\*\* is Extremely Significant ( $P < 0.01$ ); \*\* Significant ( $0.01 < P < 0.05$ ); \* More Significant ( $0.05 < P < 0.1$ ).

significant fitting ( $P < 0.01$ ), which can evaluate the parameter relationship between the test factors and the evaluation indexes.

The regression analysis of the test results was carried out by using the fitting regression model in Minitab 18. The regression equation of the evaluation index straw crushing rate (Eq. (14)) and the coefficient of variation of straw uniformity (Eq. (15)) was obtained.

$$\text{Crushing rate} = 32.79 + 3.35n_s - 4.27n_x + 6.62H_g - 3.30v \quad (14)$$

$$\begin{aligned} \text{Variation coefficient of uniformity} = & 16.88 + 0.907n_s + 1.998n_x \\ & - 0.718H_g - 1.860v \end{aligned} \quad (15)$$

Through the test, the optimal parameter combination in the process of strip application was obtained as the fourth group and the seventh group of simulation tests. In the seventh group of simulation tests, it can be seen from the above simulation analysis that when the strip application depth is 200 mm, there will be soil blocking in front of the trenching shovel. At this time, the operation resistance will increase sharply. Therefore, the operation parameters in the fourth group of simulation tests can better meet the operation quality of the breaking strip application device.

When the upper roller speed  $n_s$  is 150 r·min<sup>-1</sup>, the lower roller speed  $n_x$  is 300 r·min<sup>-1</sup>, the strip application depth  $H_g$  is 150 mm, and the forward speed is 5 km h<sup>-1</sup>, the straw crushing rate is 33.6 %. The

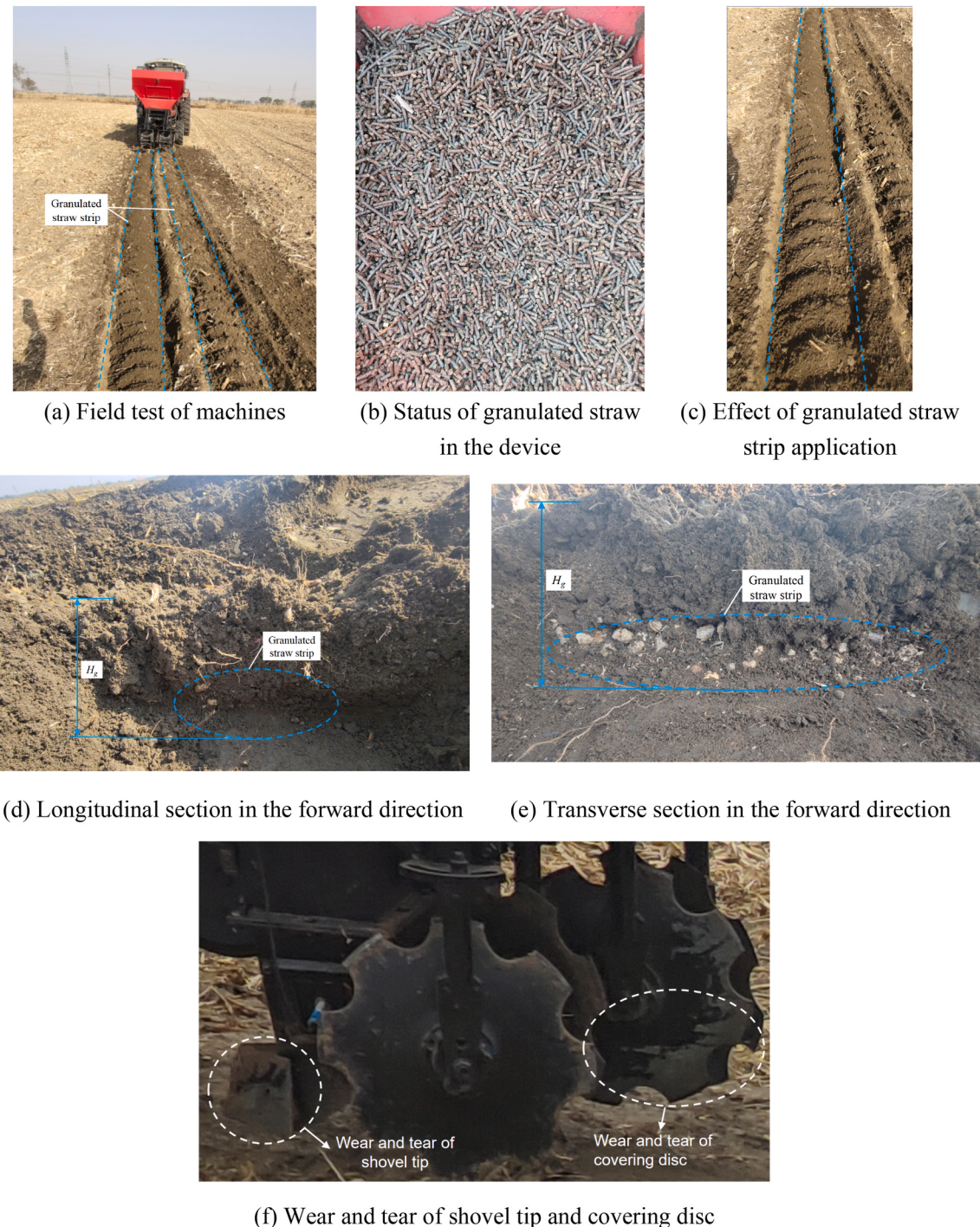


**Fig. 23.** Process and results of field strip application test.

variation coefficient of strip application uniformity is 14.4 %. In the optimisation design of operation parameters of straw crushing and strip application devices, the model of granulated straw was used to carry out simulation tests, and the above optimal operation parameters were obtained. The simulation results can provide a basis for the transmission ratio design in gear roller transmission. Ensure that the speed ratio of the upper and lower crushing rollers under the transmission of a single hydraulic motor is the optimal value after simulation optimisation. At the same time, it can reduce the manufacturing cost of the strip application device, ensure the crushing effect of granulated straw, and provide support for the precise adjustment of the operating parameters of the mechanised strip application device for granulated straw. However, there are many kinds of soil conditions in the process of granulated straw strip application, and there are significant differences in soil types, soil firmness, and moisture content of different plots (Lin et al., 2024; Liu et al., 2024). Therefore, it will be necessary to verify the applicability of the strip application device to the above types of soil.

### 3.3. Field test validation

The opening of the straw box was adjusted to 50 mm before the start of the test, and the straw in the box is shown in Fig. 23b. During the test, the forward speed of the equipment was 5 km h<sup>-1</sup>, and the forward distance of the granulated straw strip application test was 200 m (Fig. 23a–c). Samples were taken every 5 m along the strip application direction. A total of five sampling points were taken. Each sampling point selected five areas with a length of 200 mm. For the area with a width of 200 mm, the coefficient of variation was obtained by calculating the straw mass  $M_b$  of each section. The granulated straw (200 mm × 200 mm) at the section of straw strip application within the ten sampling points was collected. The sampling process of straw strip application is shown in Fig. 23c,d,e.

As shown in Fig. 24a, the average uniformity coefficient of variation of the granulated straw strip I was 14.7 %, the average uniformity coefficient of variation of strip II was 15.0 %, the average coefficient of variation of strip application was 14.9 %, and the fluctuation range was within 5.0 %. As shown in Fig. 24b, the average crushing rate of granulated straw in the strip I in the five sampling points is 40.2 %, and the average crushing rate of granulated straw in the strip II is 42.8 %, with an average value of 41.5 %. In addition, the force on the shovel tip and the edge of the covering disc of the strip application device is greater, and the wear is more severe. The wear is greater at the positions of the shovel tip and the edge of the disc. This phenomenon effectively supports the force during the simulation test. It guides the selection of wear-resistant and impact-resistant material 65Mn steel for the digging shovel tip and covering disc (Fig. 23f).

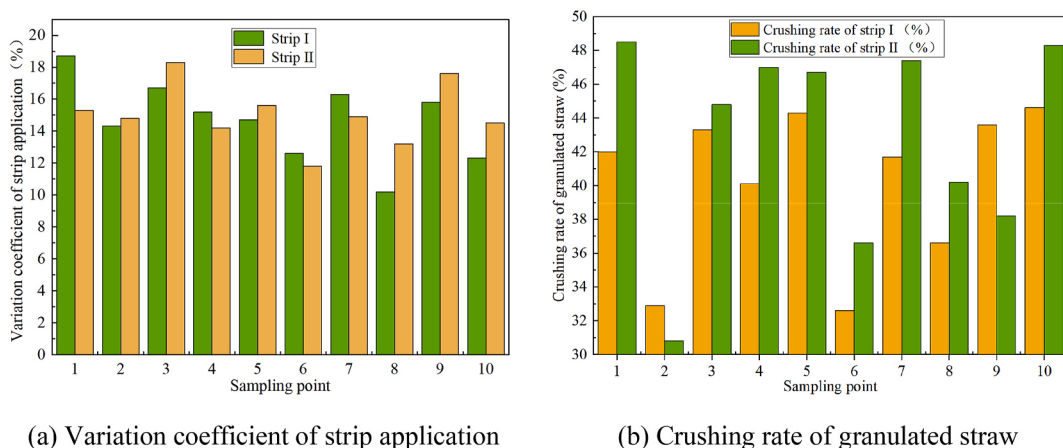
In the agronomic requirements of straw returning to the field, the

straw length is usually less than 100 mm. However, there is no specific requirement for the particle size length in the granulated straw strip application standard. In theory, the smaller the straw length, the faster the decomposition rate, the smaller the impact on subsequent sowing and emergence, and the strip application operation quality is better. Crushing the granulated straw with the roller crushing device can reduce the length of the straw and improve its uniformity. The results showed that the simulation test could better simulate the mechanised strip application process of granulated straw. The variation coefficient of strip application uniformity in the simulation test was 14.4 %, and the error between the simulation test and the field test was 0.5 %. The average crushing rate of granulated straw 33.6 %, and the error between the simulation test and the field test was 7.9 %, which could meet the requirements of mechanised strip application.

The existing traditional rigid straw modelling is added in the manuscript, which can not simulate the mechanical behaviour changes of the straw body under the action of the device in the process of straw cleaning (Chen et al., 2024), crushing (Chen et al., 2024), transportation (Li et al., 2024; Tang et al., 2023), rotary tillage (Zhao et al., 2020), mixed burial (Xie et al., 2024), and deep burial (Tong et al., 2023). This has limitations for simulating the interaction between machine and soil straw. The coupling simulation model of differential roller strip applicator flexible straw soil particles constructed in this paper can overcome this limitation and provide a new modelling idea for treating straw, organic fertiliser, and other flexible materials. At present, there is relatively little research on simulating the application of flexible granulated straw crushing strips into the soil, involving mechanical devices simultaneously interacting with flexible straw and soil particles and the interaction between straw and soil. The application process involves flexible straw crushing, trenching, soil covering, and compaction, making the operation process complex and difficult to simulate and model. In the future, simplifying simulation models can provide better simulation support for the interaction between machinery, flexible materials, and soil and further improve simulation speed.

## 4. Conclusion

Using the granulated straw model to optimise the structural and working parameters of the mechanical strip application device can reduce the development cost of the device and improve research and development efficiency. In this paper, based on the discrete element model of heterogeneous two-way bond straw, the working parameters of the strip application device were optimised and analysed to guide the field mechanised strip application process of granulated straw. The main conclusions are as follows.



(a) Variation coefficient of strip application

(b) Crushing rate of granulated straw

Fig. 24. Field validation test on the variation coefficient of strip application and crushing rate of granulated straw.

- (1) Constructed an interaction model between Machinery-Soil-Flexible straw. A differential roller-type straw particle crushing device was designed according to the agronomic requirements of mechanised strip application of granulated straw. Determine that the centre distance between the two rollers is 99 mm, the teeth height  $H$  is 15 mm, teeth width  $b_1$  is 10 mm, and teeth thickness  $b_2$  is 10 mm.
- (2) Based on the discrete element model of the granulated straw group, the straw crushing capacity of the differential counter roller was simulated, and the influence of the change of the device's operating parameters on the crushing rate was obtained. Clearly, the straw crushing rate had little difference with the flow in the range of  $0.77\text{--}1.77 \text{ kg s}^{-1}$ . When the rotation speed of the upper roller was in the range of  $100\text{--}200 \text{ r}\cdot\text{min}^{-1}$ , and the rotation speed of the lower roller was in the range of  $300\text{--}400 \text{ r}\cdot\text{min}^{-1}$ , the straw crushing rate was at a high level.
- (3) Based on the optimal parameter range of the single-factor test, the simulation model of mechanised strip application of granulated straw was constructed, and the process of mechanised strip application of granulated straw was studied by using the orthogonal test method. When the upper roller speed  $n_s$  was  $150 \text{ r}\cdot\text{min}^{-1}$ , the lower roller speed  $n_x$  was  $300 \text{ r}\cdot\text{min}^{-1}$ , the strip application depth  $H_g$  was 150 mm, and the forward speed was  $5 \text{ km h}^{-1}$ , the straw crushing rate was 33.6 %. The uniformity variation coefficient was 14.4 %, which can meet the requirements of strip application.
- (4) Field tests were conducted to verify the operation parameters obtained from the strip application process. The average variation coefficient of strip application was 14.9 %. The average crushing rate of granulated straw was 41.5 %. The error with field tests was 0.5 % and 7.9 %, which indicated that the simulation test can better simulate the mechanised strip application process of granulated straw. The optimised test parameters of the straw-crushing device can meet the requirements of mechanised strip application.
- (5) The differential counter roll device can be applied to crush other agricultural wastes to verify the device's universality. Combined with sensor technology, a real-time parameter adjustment system based on straw flow and particle size was developed to realise the dynamic optimisation of roll speed and forward speed. Over the long term, agricultural tests can be carried out for many years to analyse the beneficial effects of straw decomposition rate on soil physical and chemical properties under different crushing parameters.

#### CRediT authorship contribution statement

**Guibin Chen:** Writing – review & editing, Writing – original draft, Validation, Software, Resources, Formal analysis. **Jiaming Yang:** Writing – review & editing, Writing – original draft, Validation. **Fuzeng Yang:** Resources, Methodology. **Qingjie Wang:** Validation, Resources, Methodology, Funding acquisition. **Zhijie Liu:** Writing – review & editing, Validation, Investigation, Data curation. **Zhengdao Liu:** Resources, Methodology, Funding acquisition.

#### Declaration of competing interest

The authors declare that they have no known competing financial interests or personal relationships that could have appeared to influence the work reported in this paper.

#### Acknowledgements

This work was supported by the National Natural Science Foundation of China youth Science Foundation project (No.32501807), the Key R&D Program of Shaanxi Province (Grant No. 2025NC-YBXM-218).

Gratitude should be expressed to all the members of Conservation Tillage Research Centre.

#### References

- Aikins, K. A., Antille, D. L., Ucgul, M., Barr, J. B., Jensen, T. A., & Desbiolles, J. M. A. (2021). Analysis of effects of operating speed and depth on bentleg opener performance in cohesive soil using the discrete element method. *Computers and Electronics in Agriculture*, 187, Article 106236. <https://doi.org/10.1016/j.compag.2021.106236>
- Aikins, K. A., Ucgul, M., Barr, J. B., Jensen, T. A., Antille, D. L., & Desbiolles, J. M. A. (2021). Determination of discrete element model parameters for a cohesive soil and validation through narrow point opener performance analysis. *Soil and Tillage Research*, 213, Article 105123. <https://doi.org/10.1016/j.still.2021.105123>
- Barr, J., Desbiolles, J., Ucgul, M., & Fielke, J. M. (2020). Bentleg furrow opener performance analysis using the discrete element method. *Biosystems Engineering*, 189, 99–115. <https://doi.org/10.1016/j.biosystemseng.2019.11.008>
- Chen, G., Wang, Q., Li, W., He, J., Li, H., & Yu, C. (2021). *Design and experiment of double roller differential speed crushing fertilizer device for block organic fertilizer* (Vol. 52, pp. 65–76). *Transactions of the Chinese Society for Agricultural Machinery* (in Chinese).
- Chen, G., Wang, Q., Li, H., He, J., Lu, C., Xu, D., & Sun, M. (2023). Experimental research on a propeller blade fertilizer transport device based on a discrete element fertilizer block model. *Computers and Electronics in Agriculture*, 208, Article 107781. <https://doi.org/10.1016/j.compag.2023.107781>
- Chen, G., Wang, Q., Li, H., He, J., Wang, X., Zhang, X., & He, D. (2024). Experimental research on vertical straw cleaning and soil tillage device based on Soil-Straw composite model. *Computers and Electronics in Agriculture*, 216, Article 108510. <https://doi.org/10.1016/j.compag.2023.108510>
- Fang, M., Yu, Z., Zhang, W., Cao, J., & Liu, W. (2022). Friction coefficient calibration of corn stalk particle mixtures using Plackett-Burman design and response surface methodology. *Powder Technology*, 396, 731–742. <https://doi.org/10.1016/j.powtec.2021.10.040>
- Gong, H., Chen, Y., Wu, S., Tang, Z., Liu, C., Wang, Z., Fu, D., Zhou, Y., & Qi, L. (2022). Simulation of canola seedling emergence dynamics under different soil compaction levels using the discrete element method (DEM). *Soil and Tillage Research*, 223, Article 105461. <https://doi.org/10.1016/j.still.2022.105461>
- Hang, C., Gao, X., Yuan, M., Huang, Y., & Zhu, R. (2018). Discrete element simulations and experiments of soil disturbance as affected by the tine spacing of subsoiler. *Biosystems Engineering*, 168, 73–82.
- Hang, C., Huang, Y., & Zhu, R. (2017). Analysis of the movement behaviour of soil between subsoilers based on the discrete element method. *Journal of Terramechanics*, 74, 35–43. <https://doi.org/10.1016/j.jterra.2017.10.002>
- Hou, S., Zhu, Y., Zhu, X., Wang, Y., Ji, W., & Chen, H. (2022). Design and experiment of a straw clearing mulching no-tillage planter. *Biosystems Engineering*, 221, 69–80. <https://doi.org/10.1016/j.biosystemseng.2022.06.010>
- Leblanc, T., Smeets, B., Ramon, H., & Saeyns, W. (2016). A discrete element approach for modelling the compression of crop stems. *Computers and Electronics in Agriculture*, 123, 80–88. <https://doi.org/10.1016/j.compag.2016.02.018>
- Lee, K. S., Park, S. H., Park, W. Y., & Lee, C. S. (2003). Strip tillage characteristics of rotary tiller blades for use in a dryland direct rice seeder. *Soil and Tillage Research*, 71, 25–32. [https://doi.org/10.1016/S0167-1987\(02\)00159-9](https://doi.org/10.1016/S0167-1987(02)00159-9)
- Lenaerts, B., Aertsen, T., Tijskens, E., De Ketelaere, B., Ramon, H., De Baerdemaeker, J., & Saeyns, W. (2014). Simulation of grain-straw separation by Discrete Element Modeling with bendable straw particles. *Computers and Electronics in Agriculture*, 101, 24–33. <https://doi.org/10.1016/j.compag.2013.12.002>
- Li, C., Tang, Y., McHugh, A. D., Wu, X., Liu, M., Li, M., Xiong, T., Ling, D., Tang, Q., Liao, M., Du, S., Zhu, J., & Huang, Y. (2022). Development and performance evaluation of a wet-resistant strip-till seeder for sowing wheat following rice. *Biosystems Engineering*, 220, 146–158. <https://doi.org/10.1016/j.biosystemseng.2022.05.019>
- Li, W., Zhang, F., Luo, Z., Zheng, E., Pan, D., Qian, J., Yao, H., & Wang, X. (2024). Straw movement and flow field in a crushing device based on CFD-DEM coupling with flexible hollow straw model. *Biosystems Engineering*, 242, 140–153. <https://doi.org/10.1016/j.biosystemseng.2024.04.018>
- Lin, J., Liao, Q., Wang, X., Kang, Y., Du, W., & Zhang, Q. (2024). Exploring straw movement through the simulation of shovel-type seedbed preparation machine-straw-soil interaction using the DEM-MBD coupling method. *Computers and Electronics in Agriculture*, 226, Article 109465. <https://doi.org/10.1016/j.compag.2024.109465>
- Liu, J., Chen, Y., & Kushwaha, R. L. (2010). Effect of tillage speed and straw length on soil and straw movement by a sweep. *Soil and Tillage Research*, 109, 9–17. <https://doi.org/10.1016/j.still.2010.03.014>
- Liu, L., Wang, X., Zhang, X., Zhong, X., Wei, Z., Geng, Y., Cheng, X., Zhao, K., & Bai, M. (2023). Determination and verification of parameters for the discrete element modelling of single disc covering of flexible straw with soil. *Biosystems Engineering*, 233, 151–167. <https://doi.org/10.1016/j.biosystemseng.2023.08.001>
- Liu, G., Xia, J., Zheng, K., Cheng, J., Wang, K., Liu, Z., Wei, Y., & Xie, D. (2024). Measurement and evaluation method of farmland microtopography feature information based on 3D LiDAR and inertial measurement unit. *Soil and Tillage Research*, 236, Article 105921. <https://doi.org/10.1016/j.still.2023.105921>
- Matin, M. A., Desbiolles, J. M. A., & Fielke, J. M. (2016). Strip-tillage using rotating straight blades: Effect of cutting edge geometry on furrow parameters. *Soil and Tillage Research*, 155, 271–279. <https://doi.org/10.1016/j.still.2015.08.016>
- Saikha, S. A., Li, Y., Ma, Z., Chandio, F. A., Tunio, M. H., Liang, Z., & Solangi, K. A. (2021). Discrete element method (DEM) simulation of single grouser shoe-soil

- interaction at varied moisture contents. *Computers and Electronics in Agriculture*, 191, Article 106538. <https://doi.org/10.1016/j.compag.2021.106538>
- Shen, H., Zhang, H., Fan, J., Xu, R., & Zhang, X. (2022). Influence of contact radius on rock mechanical property and its application in discrete element method software EDEM. *Rock and Soil Mechanics*, 43, 580–590+600. <https://doi.org/10.16285/j.rsm.2020.1194>
- Shi, Y., Jiang, Y., Wang, X., Thuy, N. T. D., & Yu, H. (2023). A mechanical model of single wheat straw with failure characteristics based on discrete element method. *Biosystems Engineering*, 230, 1–15. <https://doi.org/10.1016/j.biosystemseng.2023.03.017>
- Sun, X., Niu, L., Zhang, H., Wang, Q., Zhou, W., Tang, H., & Wang, J. (2024). Exploring sustainable agriculture: Investigating the impact of controlled release fertilizer damage through bonded particle modeling. *Journal of Cleaner Production*, 468, Article 143095. <https://doi.org/10.1016/j.jclepro.2024.143095>
- Tang, H., Xu, W., Zhao, J., Xu, C., & Wang, J. (2023). Comparison of rice straw compression characteristics in vibration mode based on discrete element method. *Biosystems Engineering*, 230, 191–204. <https://doi.org/10.1016/j.biosystemseng.2023.04.009>
- Tong, Z., Li, H., He, J., Wang, Q., Lu, C., Wang, C., Zhong, G., Cui, D., & Li, D. (2023). Design and experiment of in situ soil-lifting shovel for direct-injection straw deep-burial machine. *Agriculture*, 13, 1650. <https://doi.org/10.3390/agriculture13091650>
- Torotwa, I., Ding, Q., Makange, N. R., Liang, L., & He, R. (2021). Performance evaluation of a biomimetically designed disc for dense-straw mulched conservation tillage. *Soil and Tillage Research*, 212, Article 105068. <https://doi.org/10.1016/j.still.2021.105068>
- Ucgul, M., Saunders, C., Li, P., Lee, S., & Desbiolles, J. M. A. (2018). Analyzing the mixing performance of a rotary spader using digital image processing and discrete element modelling (DEM). *Computers and Electronics in Agriculture*, 151, 1–10. <https://doi.org/10.1016/j.compag.2018.05.028>
- Wang, X., Gao, P., Yue, B., Shen, H., Fu, Z., Zheng, Z., Zhu, R., & Huang, Y. (2019). Optimisation of installation parameters of subsoiler' wing using the discrete element method. *Computers and Electronics in Agriculture*, 162, 523–530. <https://doi.org/10.1016/j.compag.2019.04.044>
- Wang, Y., Li, N., Ma, Y., Tong, J., Pfleging, W., & Sun, J. (2020). Field experiments evaluating a biomimetic shark-inspired (bios) subsoiler for tillage resistance reduction. *Soil and Tillage Research*, 196, Article 104432.
- Wang, X., Lv, G., Zhang, Y., Yu, Y., Wang, X., Peixoto, L., Qian, C., & Pang, H. (2023). Annual burying of straw after pelletizing: A novel and feasible way to improve soil fertility and productivity in Northeast China. *Soil and Tillage Research*, 230, Article 105699. <https://doi.org/10.1016/j.still.2023.105699>
- Wang, X., Yang, H., Liu, J., Wu, J., Chen, W., Wu, J., Zhu, L., & Bian, X. (2015). Effects of ditch-buried straw return on soil organic carbon and rice yields in a rice-wheat rotation system. *Catena*, 127, 56–63. <https://doi.org/10.1016/j.catena.2014.10.012>
- Xie, D., He, J., Liu, T., Liu, C., Zhao, G., & Chen, L. (2024). Establishment and validation of the DEM-MBD coupling model of flexible straw-Shajiang black soil-walking mechanism interactions. *Computers and Electronics in Agriculture*, 224, Article 109203. <https://doi.org/10.1016/j.compag.2024.109203>
- Zhang, S., Zhao, H., Wang, X., Dong, J., Zhao, P., Yang, F., Chen, X., Liu, F., & Huang, Y. (2023). Discrete element modeling and shear properties of the maize stubble-soil complex. *Computers and Electronics in Agriculture*, 204, Article 107519. <https://doi.org/10.1016/j.compag.2022.107519>
- Zhao, H., Li, H., Ma, S., He, J., Wang, Q., Lu, C., Zheng, Z., & Zhang, C. (2020). The effect of various edge-curve types of plain-straight blades for strip tillage seeding on torque and soil disturbance using DEM. *Soil and Tillage Research*, 202, Article 104674. <https://doi.org/10.1016/j.still.2020.104674>
- Zhu, D., Shi, M., Yu, C., Yu, Z., Kuang, F., Xiong, W., & Xue, K. (2023). Tool-straw-paddy soil coupling model of mechanical rotary-tillage process based on DEM-FEM. *Computers and Electronics in Agriculture*, 215, Article 108410. <https://doi.org/10.1016/j.compag.2023.108410>